Efficient Quantization for Overcomplete Expansions in $\mathbb{R}^N$

Baltasar Beferull-Lozano, *Student Member, IEEE,* and Antonio Ortega, *Senior Member, IEEE*

***Abstract*—In this paper, we study construction of structured regular quantizers for overcomplete expansions in $\mathbb{R}^N$. Our goal is to design structured quantizers which allow simple reconstruction algorithms with low complexity and which have good performance in terms of accuracy. Most related work to date in quantized redundant expansions has assumed that the same uniform scalar quantizer was used on all the expansion coefficients. Several approaches have been proposed to improve the reconstruction accuracy, with some of these methods having significant complexity. Instead, we consider the joint design of the overcomplete expansion and the scalar quantizers (allowing different step sizes) in such a way as to produce an equivalent vector quantizer (EVQ) with periodic structure. The construction of a periodic quantizer is based on lattices in $\mathbb{R}^N$ and the concept of geometrically scaled-similar sublattices. The periodicity makes it possible to achieve good accuracy using simple reconstruction algorithms (e.g., linear reconstruction or a small lookup table).**

***Index Terms*—Consistency, intersection lattice, overcomplete expansions, periodic quantizers, tight frames.**

I. Introduction and Motivation

QUANTIZED redundant expansions are useful in different applications such as oversampled analog-to-digital (A/D) conversion of band-limited signals [1]–[5] and multiple-description quantization [6], [7], [36], [37]. In the first case, the purpose of using redundant expansions is to attain accurate digital signal representations under scenarios where the cost of using high-rate quantization is much higher than that of having a high oversampling or redundancy. The most important case is the A/D conversion of band-limited signals, where in order to use high-rate quantization to discretize the amplitude it is necessary to use expensive high-precision analog circuitry. Instead, accuracy is attained by performing oversampling and exploiting this redundancy to reduce the loss of information caused by low-resolution quantization. Some other systems have been proposed in the context of pattern recognition for images, where overcomplete transforms are used to emulate the human visual system, which has a high degree of oversampling in orientation and scale [8], [9]. Moreover, an increase in resolution due to angular oversampling in the frequency domain has been observed experimentally for quantized (two-dimensional (2-D)) steerable transforms [10], so that increasing the number of orientations yields a gain in energy compaction [11]. Quantized overcomplete expansions also arise in the context of joint source–channel coding for erasure channels [6], [7], [36], [37].

There are two major factors that determine the accuracy that can be attained using quantized overcomplete expansions: the reconstruction algorithm and the quantization scheme. There has been extensive research work aiming at finding reconstruction algorithms that are optimal or near optimal in terms of asymptotic (large redundancy values) accuracy. However, the quantization scheme has been always assumed to be a uniform scalar quantization with the same step size for all expansion coefficients. In this paper, we explore efficient quantization designs for overcomplete expansions.

Reconstruction algorithms have been studied following two main approaches. The first one is based on modeling the quantization noise as an additive white noise uncorrelated with the signal that is quantized. These models are sometimes convenient for analysis and lead to useful results in some scenarios [12], [13]. It can be shown that if a white-noise model is assumed for the scalar quantization noise of the coefficients and the same step size is used to quantize all the coefficients, the optimal reconstruction is given by the usual linear reconstruction [14], where linear reconstruction consists of first projecting the signal into a set of vectors (with cardinal larger than the dimension), obtaining a set of coefficients, and then reconstructing by taking a simple weighted average of these coefficients. Thus, in practice, linear reconstruction is always used when the assumptions leading to this analysis are valid. In the context of tight frames, an important class of overcomplete expansions, theoretical analysis shows (under this quantization scheme and stochastic model) that linear reconstruction [14] gives a reduction in the power of each noise component (quantization noise of each projection or coefficient) that is proportional to the redundancy r of the tight frame. The same decay of the mean square error (MSE) in the signal domain can be shown theoretically in the cases of tight frames in $\mathbb{R}^N$, Weyl–Heisenberg frames in $\ell^2(\mathbb{Z})$, and in classical oversampled A/D conversion with uniform sampling and linear reconstruction (tight sinc frames) where MSE $= \frac{\Delta^2}{12r}$ [12]. The behavior of the MSE $= O(1/r)$ is observed experimentally when uniform quantization with the

Manuscript received May 11, 2001; revised September 14, 2002. This work was supported in part by the National Science Foundation under Grant MIP-9804959, a Ph.D. Fellowship from the Ministry of Education and Science of Spain, and the Integrated Media Systems Center, a National Science Foundation Engineering Research Center. The material in this paper was presented in part at the IEEE Data Compression Conference, Snowbird, UT, March 2001 and at the International Conference on Acoustics, Speech and Signal Processing, Salt Lake City, UT, May 2001.

B. Beferull-Lozano was with the Department of Electrical Engineering-Systems, University of Southern California, Los Angeles, CA 90089-2564 USA. He is now with the Swiss Federal Institute of Technology–EPFL, Lausanne, CH-1015, Switzerland (e-mail: baltasar.beferul@epfl.ch).

A. Ortega is with the Department of Electrical Engineering-Systems, University of Southern California, Los Angeles, CA 90089-2564 USA (e-mail: ortega@sipi.usc.edu).

Communicated by P. A. Chou, Associate Editor for Source Coding.

Digital Object Identifier 10.1109/TIT.2002.806117

same step size is used and the step size is small enough so that the white-noise model approximately applies. One of the reasons for linear reconstruction not to be optimal in some cases is that the reconstructed signal may not be consistent with the original signal in the sense that the output obtained from requantizing the reconstructed signal is different than the output obtained when quantizing the original signal, implying a larger reconstruction error on average. On the other hand, it has not been studied whether using a more intelligent quantization system allowing in general different step sizes to quantize the coefficients can lead to improvements in the rate-distortion performance when reconstructing with a linear reconstruction algorithm. This is one of the issues that is addressed in this paper.

The second approach is completely based on a deterministic analysis of the quantization noise. This deterministic approach was introduced by Thao and Vetterli [4] and later extended in [1], [3], [5]. This deterministic analysis based on hard bounds of the quantization noise led to two nonlinear reconstruction algorithms for frames in $\mathbb{R}^N$, one based on projection on convex sets (POCS) theory [15], [4], [17], [18] and the other one based on linear programming (LP) [5]. The main result is that these reconstruction algorithms ensure that the reconstruction vector falls always inside the same cell as the input vector. These reconstructions are called *consistent* and in quantization terms this means that the equivalent quantizer is regular. It was observed experimentally that for high enough redundancies r and for uniform quantization of all the frame coefficients consistent reconstruction algorithms have an asymptotic MSE behavior of $O(1/r^2)$. Moreover, Thao and Vetterli proved (under some mild conditions) that consistency guarantees this asymptotic behavior for high enough redundancies r for the case of oversampled A/D conversion of T-periodic band-limited continuous-time signals, which can be viewed as a frame expansion in $\mathbb{R}^N$ with respect to a certain discrete Fourier transform (DFT)-like frame. Later, Cvetković [1], [2] proved this fact under some mild restrictions for overcomplete expansions in $\mathbb{R}^N$ in general. Cvetković proposed a more efficient reconstruction algorithm called *semilinear reconstruction algorithm* which also attains asymptotically an accuracy of $O(1/r^2)$ without satisfying consistency. This algorithm is based on the positions of the threshold crossings and identifying a good linear system to solve. Moreover, Cvetković and Daubechies extended this idea to be used in the context of single-bit oversampled A/D conversion where a deterministic dither is used in order to force threshold-crossing locations with certain properties which allow exponential accuracy in the bit rate [16]. Recently, Rangan and Goyal [19] have proposed a recursive algorithm using subtractive dithered quantization which also attains asymptotically an accuracy of $O(1/r^2)$, again, without ensuring consistency.

The crucial observation that motivates our work is that in all the previous work a very simple quantization scheme has been assumed which requires sophisticated reconstruction algorithms [15], [4], [17]–[19], [1], [2] in order to improve its accuracy with respect to the classic approach [14] (simple quantization and linear reconstruction). Instead, in this paper, we pose the following question: are there quantization schemes where there is no difference in performance between using simple reconstruction algorithms (e.g., linear or of similar complexity) and more sophisticated reconstruction methods? Although all the improved reconstruction algorithms that have been proposed so far can achieve very good accuracy, the computational complexity of these methods (although different in each case), for a given redundancy is higher than that of linear reconstruction [5], [4]. Since simple reconstructions (e.g., linear or lookup table) are normally preferable in practical scenarios, in our work we assume that a simple reconstruction will be used and the main focus is to explore whether better quantization designs, e.g., using different step sizes, may have the advantage of achieving a performance which is superior with respect to simple quantization methods, e.g., using the same step size. In other words, our goal is to provide the tools to design the overcomplete expansions and the corresponding quantization system so that the overall system behaves like a regular quantizer and achieves the best possible performance using simple reconstruction algorithms. Designing the quantization system with a structure that forces consistency, using the usual linear reconstruction, may result in worse performance, in terms of rate distortion, than a *different* system whose structure results in inconsistency. However, we will show that because of the periodic structure of the quantization system, very simple reconstruction techniques (e.g., those based on a lookup table) can be designed which significantly outperform linear reconstruction.

The fundamental idea that we use in order to achieve this goal is to design jointly the overcomplete expansion together with the quantization system by choosing carefully the step sizes of the scalar quantizers so that the whole system is equivalent to a vector quantizer in $\mathbb{R}^N$ with a periodic structure. First, we define an equivalent vector quantizer (EVQ) given a quantization scheme and a reconstruction algorithm. Then, based on this equivalence, we introduce the concept of periodic quantizers and show how to construct and design periodic quantizers. This periodic structure can be conveniently characterized and parameterized in terms of lattices and sublattices. Next, we explain the advantages that are provided by this periodic structure and show how the periodic structure in the EVQ is a necessary condition to achieve consistency under the usual linear reconstruction. Once a periodic structure is present, the number of different cells of this vector quantizer becomes finite and although a sufficient condition cannot be expressed formally, it is very simple to check whether consistency is satisfied or not. For a given family of vectors and a set of different step sizes which yield a periodic vector quantizer in $\mathbb{R}^N$, it is possible to reconstruct by using a small lookup table, where the reconstruction vectors can be chosen to be the centroids of the cells with respect to a uniform distribution. Moreover, it is also possible to design systems such that the EVQ has some additional symmetry which allows to use a very simple improved linear reconstruction. Our system provides excellent performance while having the same complexity as linear reconstruction, but is more suitable to be used in $\mathbb{R}^N$ for low to moderate values of the dimension N and for low values of redundancy [20], [21]. Although we present examples and results for small redundancies, it is clearly shown that the basic theoretical idea of periodicity can be extended to higher redundancies and that the problem of finding good quantizers with higher redundancies consists of searching for good lattices and

sublattices with certain properties. Extensions to higher dimensions have been analyzed by Sloane and Beferull-Lozano recently and can be found in [22]. On the other hand, although we believe that multiple description coding is also a potential application of our framework, we have not explored this application in this paper.

This paper is organized as follows. In Section II, we define the EVQ and the property of consistency. Section III describes the construction and design of periodic quantizers in terms of lattices. In Section IV, it is first shown that the periodic structure in the EVQ is a necessary condition to achieve consistency under the usual linear reconstruction, and then, low-complexity reconstruction schemes in periodic quantizers are analyzed. Finally, numerical results for some specific designs in $\mathbb{R}^2$ are shown in Section V as well as a simple direct application of our designs in $\mathbb{R}^2$ to oversampled A/D conversion of sinusoid signals.

II. Linear Reconstruction, Equivalent Vector Quantizer, and Consistency

In this section, we first review the basic concept of a tight frame in $\mathbb{R}^N$, and express a linear reconstruction in terms of an EVQ, which can be parameterized in terms of lattices.

A. Linear Reconstruction in Tight Frames Without Quantization

For the sake of clarity, we review briefly the definitions and main properties of tight frames.

Definition 1: Let $\Phi = \{\boldsymbol{\varphi}_i\}_{i=1}^M \subset \mathbb{R}^N$ where $\|\boldsymbol{\varphi}_i\| = 1$, $\forall i = 1, \ldots, M$. Φ is called a frame if there exist $A > 0$, and $A \leq B < \infty$ such that

$$A\|\boldsymbol{x}\|^2 \leq \sum_{i=1}^{M} |\langle \boldsymbol{x}, \boldsymbol{\varphi}_i\rangle|^2 \leq B\|\boldsymbol{x}\|^2, \qquad \forall \boldsymbol{x} \in \mathbb{R}^N. \tag{1}$$

A and B are called lower and upper frame bounds. Given a frame Φ, the associated frame operator $\boldsymbol{F}$: $\mathbb{R}^N \longrightarrow \mathbb{R}^M$ is given by an $M \times N$ matrix defined as

$$\begin{aligned} \boldsymbol{F} &= (\boldsymbol{\varphi}_1 \boldsymbol{\varphi}_2 \cdots \boldsymbol{\varphi}_M)^T \\ \boldsymbol{y}_i &= (F\boldsymbol{x})_i = \langle \boldsymbol{x}, \boldsymbol{\varphi}_i\rangle = \boldsymbol{\varphi}_i^T \boldsymbol{x}, \qquad \forall \boldsymbol{x} \in \mathbb{R}^N. \end{aligned} \tag{2}$$

Definition 2: The minimal dual frame of Φ is defined as $\tilde{\Phi} = \{\tilde{\boldsymbol{\varphi}}_i\}_{i=1}^M$ where

$$\tilde{\boldsymbol{\varphi}}_i = \left(\boldsymbol{F}^T\boldsymbol{F}\right)^{-1} \boldsymbol{\varphi}_i, \qquad \forall i = 1, \ldots, M. \tag{3}$$

Definition 3: A frame Φ is called a tight frame if $A = B$, that is, if the lower and upper bounds are equal.

The following properties are satisfied for a tight frame.

1) The minimal dual frame $\tilde{\Phi}$ of a tight frame Φ is given by

$$\tilde{\boldsymbol{\varphi}}_i = \frac{1}{r}\boldsymbol{\varphi}_i, \qquad \forall i = 1, \ldots, M \text{ with } r = \frac{M}{N} \tag{4}$$

and the redundancy r of the tight frame is equal to the frame bounds, that is, $r = A = B$.

2) $\forall \boldsymbol{x} \in \mathbb{R}^N$, the expansion with respect to the frame $\boldsymbol{\Phi} = \{\boldsymbol{\varphi}_i\}_{i=1}^M$ whose coefficients have the minimum possible norm (most economical expansion) is given by

$$\boldsymbol{x} = \sum_{i=1}^{M} \langle \boldsymbol{x}, \tilde{\boldsymbol{\varphi}}_i\rangle \boldsymbol{\varphi}_i = \frac{1}{r}\sum_{i=1}^{M} \langle \boldsymbol{x}, \boldsymbol{\varphi}_i\rangle \boldsymbol{\varphi}_i. \tag{5}$$

In this section, we restrict the discussion to the case of tight frames that are composed by a set of $r > 1$ different orthogonal bases. This is done without loss of generality for purposes of clarity because the geometric analysis is much simpler. Extensions to generic frames are simple and can be obtained by using in the reconstruction the corresponding dual frames, which will be different in each case. With this restriction, we can group the vectors $\{\boldsymbol{\varphi}_i\}_{i=1}^M$ that compose the tight frame as $\{\{\boldsymbol{\varphi}_i^j\}_{i=1}^N\}_{j=1}^r$, where $\{\boldsymbol{\varphi}_i^j\}_{i=1}^N$ is the jth basis.

Remark on Notation: In this paper, we make an extensive use of superscripts and subscripts. For instance, in a tight frame composed of r orthogonal bases, the superscript $j \in \mathbb{Z}_+$ indicates the jth basis and the subscript i indicates the ith vector of the jth basis. Also, in order to avoid confusion with the superscripts, to represent a number b raised to the power of e (e being any real number), we will use $(b)^e$, and we will use b^e for indexation (eth element), with $e \in \mathbb{Z}_+$.

For the sake of simplicity, we restrict most of the equations and expressions of this section, without any loss of generality, to the case of $\mathbb{R}^2$. For $N = 2$, the frame contains $M = 2r$ unitary vectors that form r orthogonal bases and the frame operator can be written as $\boldsymbol{F} = [\boldsymbol{\varphi}_1^1\boldsymbol{\varphi}_2^1\boldsymbol{\varphi}_1^2\boldsymbol{\varphi}_2^2 \cdots \boldsymbol{\varphi}_1^r\boldsymbol{\varphi}_2^r]^T$. If we define each orthogonal matrix $\boldsymbol{F}^j$ as $\boldsymbol{F}^j = [\boldsymbol{\varphi}_1^j\boldsymbol{\varphi}_2^j]^T$, then we call $\boldsymbol{y}^j = [y_1^j, y_2^j]^T$ the 2-D vector of coefficients associated with the jth basis, which is given by $\boldsymbol{y}^j = \boldsymbol{F}^j\boldsymbol{x}$. The M-dimensional vector of coefficients $\boldsymbol{y} = \boldsymbol{F}\boldsymbol{x}$ will be expressed as $\boldsymbol{y} = [y_1^1, y_2^1, y_1^2, y_2^2, \ldots, y_1^r, y_2^r]^T$.

B. EVQ for Linear Reconstruction

Assume that scalar quantization is applied to the frame coefficients. Let SQ_i^j be a uniform scalar quantizer with step size Δ_i^j and decision points $\{m\Delta_i^j\}_{m\in\mathbb{Z}}$. This is a particular choice without any loss of generality, that is, what follows is also valid for scalar quantizers with decision points $\{(m + \frac{1}{2})\Delta_i^j\}_{m\in\mathbb{Z}}$ where 0 is a reconstruction point.

Then, we define $SQ_1^1 \times SQ_2^1 \times \cdots \times SQ_1^r \times SQ_2^r$ as an M-dimensional product scalar quantizer (PSQ) applied to the M-dimensional vector of coefficients $\boldsymbol{y}$, i.e., each of the components of the vector $\boldsymbol{y}$ are quantized by a corresponding scalar quantizer (see Fig. 1).

Given a tight frame Φ and a PSQ, we define the following quantizer.

Definition 4: A quantizer Q^j, $1 \leq j \leq r$ consists of the following.

1) A set C^j of rectangular quantization cells induced by the scalar uniform quantizers $\{SQ_1^j, SQ_2^j\}$ which are applied to the frame coefficients associated with the jth basis.

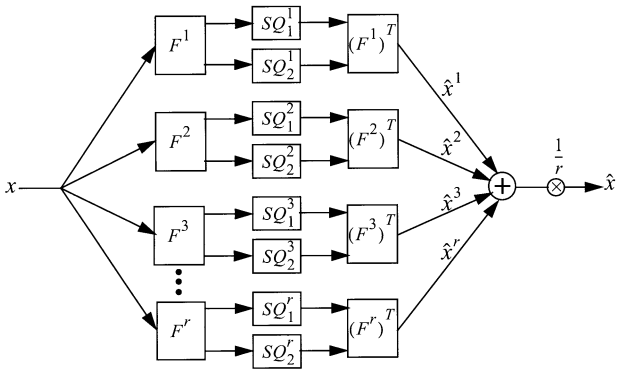

Fig. 1. Definition of the EVQ in $\mathbb{R}^2$ for a tight frame based on the linear reconstruction given by the minimal dual frame. A similar definition for the EVQ can be given for any general linear reconstruction algorithm.

2) A mapping $\mathbb{Z}^2 \longrightarrow \mathbb{R}^2$ from the set of cells C^j to a set of reconstructions (outputs) O^j such that $\forall\, \boldsymbol{x}$ satisfying

$$m_i\Delta_i^j \le SQ_i^j(\langle \boldsymbol{x}, \boldsymbol{\varphi}_i^j\rangle) \le (m_i+1)\Delta_i^j, \qquad i=1,2$$

the reconstruction vector is given by

$$\hat{\boldsymbol{x}}^j = Q^j(\boldsymbol{x}) = \sum_{i=1}^{2} SQ_i^j\Big(\Big\langle \boldsymbol{x}, \boldsymbol{\varphi}_i^j\Big\rangle\Big)\boldsymbol{\varphi}_i^j$$

$$SQ_i^j(\beta) = \left(\left\lfloor \frac{\beta}{\Delta_i^j}\right\rfloor + \frac{1}{2}\right)\Delta_i^j$$

$$\Longrightarrow\ \hat{\boldsymbol{x}}^j = \sum_{i=1}^{2}\left(m_i+\frac{1}{2}\right)\Delta_i^j\boldsymbol{\varphi}_i^j. \tag{6}$$

The step size associated with the scalar quantizer SQ_i^j is denoted by Δ_i^j. The vertices of the cells C^j form what is called a real 2-D lattice.

Definition 5: An N-dimensional lattice Λ is a discrete subgroup of $\mathbb{R}^N$ which is defined as the set of points obtained by taking integral linear combinations of N linearly independent vectors

$$\Lambda = \{\boldsymbol{x}\colon \boldsymbol{x} = u_1\boldsymbol{a}_1 + u_2\boldsymbol{a}_2 + \cdots + u_N\boldsymbol{a}_N, \quad u_i \in \mathbb{Z},\ i=1,\ldots,N\}. \tag{7}$$

The set of vectors $\{\boldsymbol{a}_i\}_{i=1}^N$ are the generator (basis) vectors of the lattice and the matrix $\boldsymbol{M}_\Lambda = (\boldsymbol{a}_1|\boldsymbol{a}_2|\cdots|\boldsymbol{a}_N)^T$ is called the generator matrix of the lattice. Thus, the vertices of the cells C^j form a lattice Λ^j having generator matrix

$$\boldsymbol{M}_{\Lambda^j} = (\Delta_1^j\boldsymbol{\varphi}_1^j|\Delta_2^j\boldsymbol{\varphi}_2^j)^T.$$

Because of the orthogonality, the basis vectors of the lattice point in the same directions as the unitary vectors that compose $\boldsymbol{F}^j$, but in general, it is clear that this is not the case when the tight frame is not composed by a set of orthogonal bases, as we will see in Section III. There are an infinite number of possible (minimal) bases that can be used for this lattice. We will always use, as a basis for the lattice Λ^j, the jth orthogonal basis $\{\boldsymbol{\varphi}_1^j, \boldsymbol{\varphi}_2^j\}$. In this way, the outputs of quantizer Q^j can be expressed directly in terms of the generator matrix $\boldsymbol{M}_{\Lambda^j}$. Notice that the cells associated with the quantizer Q^j are convex polytopes whose vertices are all in the lattice Λ^j.

Given a set of quantizers Q^j, $j=1,\ldots,r$, defined as above, we now introduce the concept of EVQ as follows.

Definition 6: An EVQ consists of the following.

1) A set of quantization cells formed by the intersection of the rectangular cells $\{C^j\}_{j=1}^r$ of the quantizers $\{Q^j\}_{j=1}^r$.
2) A mapping $\mathbb{R}^2 \longrightarrow \mathbb{R}^2$ from the set of cells to a set of reconstructions given by

$$\hat{\boldsymbol{x}} = \frac{1}{r}\sum_{j=1}^{r}\hat{\boldsymbol{x}}^j, \qquad \text{where } \hat{\boldsymbol{x}}^j = Q^j(\boldsymbol{x}). \tag{8}$$

Thus, the linear reconstruction, as represented in Fig. 1 and shown in Fig. 2(b), consists of taking the geometrical average point among the different reconstructions $\hat{\boldsymbol{x}}^j$, $j=1,\ldots,r$.

The PSQ in $\mathbb{R}^M$ leads to an EVQ in $\mathbb{R}^2$ and the output of the EVQ can be written as a linear combination of the outputs from each 2-D quantizer Q^j where it can be seen that the set of outputs (reconstructions) of quantizer Q^j forms a coset of the lattice Λ^j. Fig. 2(a) illustrates the partition generated by the EVQ for an example where $r=2$, and the tight frame and associated step sizes are

$$\boldsymbol{F} = \begin{pmatrix} 1 & 0 \\ 0 & 1 \\ \cos\left(\frac{\pi}{6}\right) & \sin\left(\frac{\pi}{6}\right) \\ -\sin\left(\frac{\pi}{6}\right) & \cos\left(\frac{\pi}{6}\right) \end{pmatrix}$$

$$\Delta_2^1 = \frac{6}{5}\Delta_1^1 \quad \Delta_1^2 = \frac{13}{10}\Delta_1^1 \quad \Delta_2^2 = \frac{9}{8}\Delta_1^1. \tag{9}$$

Fig. 2(b) illustrates how the final reconstruction vector $\hat{\boldsymbol{x}}$ is obtained. Notice that since the cells C^j generated by the quantizer Q^j are convex polytopes, the cells $C^{\mathrm{EVQ}} = C^{\Lambda^1} \cap \cdots \cap C^{\Lambda^r}$ corresponding to the EVQ are intersections of convex polytopes, and therefore are also convex polytopes in $\mathbb{R}^2$. It is important to notice that in general the EVQ is not necessarily a *Voronoi or nearest neighbor* vector quantizer, and although its cells are convex polytopes, they are not in general (minimum distance) Voronoi cells. For a cell to be a Voronoi cell, it would be required that any point contained in that cell be closer to the centroid of that cell than to the centroid of any other cell. This is not satisfied in general because these cells are obtained as the intersection of cells of the (nearest neighbor) quantizers $\{Q^j\}_{j=1}^r$ used in each of the basis, rather than as the nearest neighbor regions for each reconstruction vector. In other words, the intersection of nearest neighbor quantizers does not result in general in a nearest neighbor quantizer. Therefore, we will refer to EVQ cells instead of Voronoi cells. In general, for a given redundancy r, $\hat{\boldsymbol{x}}$ is obtained by averaging over the r linear reconstructions $\hat{\boldsymbol{x}}^j$ $j=1,\ldots,r$ given by the corresponding quantizers Q^j $j=1,\ldots,r$.

Remark: The concept of EVQ can be actually defined for any reconstruction algorithm, not necessarily only for the linear

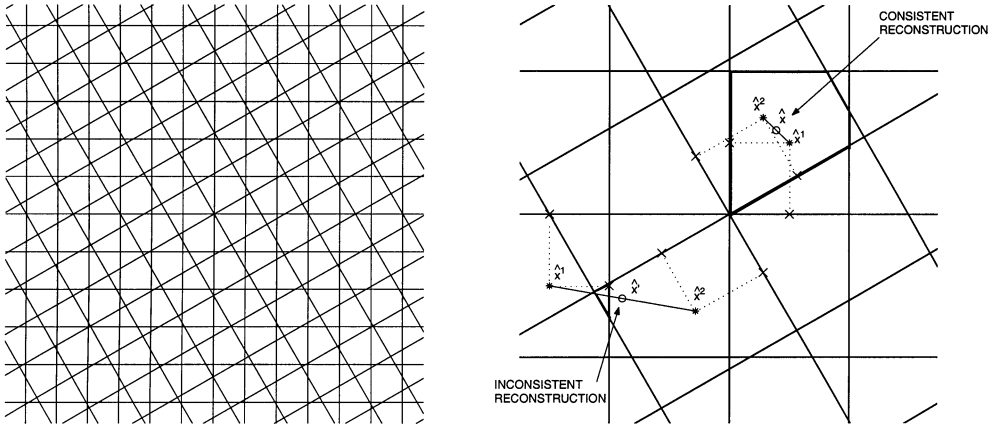

(a) (b)

Fig. 2. (a) Example of the convex polytopes C^{EVQ} in $\mathbb{R}^2$, (b) (Zoom) Example of outputs for the quantizers Q^1, Q^2, and the EVQ when linear reconstruction is used. The partial reconstructions $\hat{\boldsymbol{x}}^j$, $j = 1, 2$ are represented by "$*$" and the final reconstruction $\hat{\boldsymbol{x}}$ is represented by "$\circ$." The final reconstructions are obtained by taking the halfway point between $\hat{\boldsymbol{x}}^1$ and $\hat{\boldsymbol{x}}^2$, that is, $\hat{\boldsymbol{x}} = \frac{1}{2}(\hat{\boldsymbol{x}}^1 + \hat{\boldsymbol{x}}^2)$. Two reconstructions are shown, each reconstruction corresponding to the case where the original vector $\boldsymbol{x}$ is in each of the two EVQ cells indicated with the bold line. $\hat{\boldsymbol{x}}$ is a consistent reconstruction and $\hat{\boldsymbol{x}}'$ is an inconsistent reconstruction.

reconstruct ion algorithm using the minimal dual frame as described above. However, for clarity, we have restricted in this section the definition and concepts to this particular case. For any other reconstruction algorithm, Definitions 4 and 6 should be modified so that the set of reconstruction vectors are the ones given by the particular reconstruction algorithm that is used.

Another concept that will be used in some of the next sections is the concept of fundamental polytope. The fundamental polytope C_o^j associated with the lattice Λ^j is defined by

$$C_o^j = \left\{ \boldsymbol{x} \colon \boldsymbol{x} = \alpha_1 \Delta_1^j \boldsymbol{\varphi}_1^j + \alpha_2 \Delta_2^j \boldsymbol{\varphi}_2^j, \quad 0 \le \alpha_i < 1,\ i = 1, 2 \right\} \tag{10}$$

which is the parallelopiped formed by the basis vectors of the lattice Λ^j. The area of this fundamental polytope is equal to $|\det(\boldsymbol{M}_{\Lambda^j})|$.

C. Property of Consistency for a Generic Reconstruction Algorithm

Although the concept of consistency was introduced in [4], for the sake of clarity and because it is a central concept for this paper, we review it here. Given a tight frame $\boldsymbol{\Phi}$, constructed by using $r > 1$ orthogonal bases, it is desirable to design an EVQ such that if $\boldsymbol{x}$ is the original vector and $\hat{\boldsymbol{x}}$ is the reconstructed vector, both $\boldsymbol{x}$ and $\hat{\boldsymbol{x}}$ fall in the same EVQ cell. The reconstruction vectors $\hat{\boldsymbol{x}}$ satisfying this property are called consistent reconstructions of $\boldsymbol{x}$.

Given a frame operator F and a generic PSQ, the concepts of consistency and linear consistency for an EVQ cell C_i^{EVQ}, are defined as follows.

Definition 7 (Consistent Cell): Let C_i^{EVQ} be a cell in an EVQ, and $\hat{\boldsymbol{x}}$ its reproduction vector. C_i^{EVQ} is said to be consistent if $\hat{\boldsymbol{x}} \in C_i^{\mathrm{EVQ}}$.

For the particular case of using a linear reconstruction, the definition of linearly consistent cell is as follows.

Definition 8 (Linearly Consistent Cell): Let C_i^{EVQ} be a cell of an EVQ. C_i^{EVQ} is said to be linearly consistent if it is consistent under linear reconstruction, where the linear reproduction vector is given by $\hat{\boldsymbol{x}} = \frac{1}{r}\sum_{j=1}^{r} \hat{\boldsymbol{x}}^j$.

Remark: As before, the definition of linear consistency can be extended to any general linear reconstruction algorithm, not just the linear reconstruction given by the minimal dual frame.

An EVQ is said to be consistent if and only if all its cells C^{EVQ} are consistent. Similarly, a general reconstruction algorithm that gives rise to a consistent quantizer is called a consistent reconstruction algorithm. In particular, a quantizer which satisfies consistency under linear reconstruction is said to be linearly consistent.

Given an EVQ, the optimal reconstruction for any cell is obviously inside that cell, that is, the optimal reconstruction is always a consistent reconstruction.[1] Since an inconsistent reconstruction $\hat{\boldsymbol{x}}$ is outside the cell corresponding to the original signal $\boldsymbol{x}$, as opposed to a consistent reconstruction, consistent reconstructions will yield smaller squared distortion (MSE) than inconsistent reconstructions on average for a given EVQ. In our work, the goal is to find a set of EVQs for which it is possible to have consistent reconstructions with simple reconstruction algorithms.

Fig. 2(b) shows examples of both consistent and inconsistent cells assuming linear reconstruction. One of our goals in this paper is to design quantization techniques such that all EVQ cells are linearly consistent. Fig. 3(a) and (b) provides a simple and intuitive example that illustrates how linearly consistent EVQ cells can be achieved *by choosing scalar quantizers with different step sizes for each of the $r = 2$ bases*. It can be seen in Fig. 3(b) how the intersection between cells of Q^1 and cells of Q^2 is the same across all the partition of the EVQ. As will be explained later, the crucial idea on how to achieve consistency with low-complexity reconstruction algorithms is to enforce a *periodic* structure on the partition defined by the EVQ, as in the example of Fig. 3. Intuitively, the step sizes selected will depend

[1]This statement holds because the EVQ cells are convex.

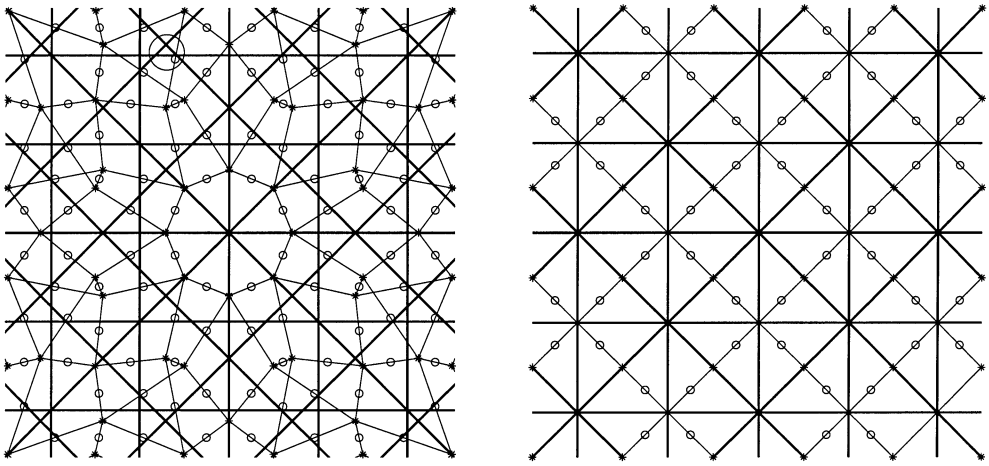

(a) (b)

Fig. 3. Example for $r = 2$ showing how the consistency problem can be solved by choosing carefully a certain frame and a set of different step sizes: (a) using the same step sizes gives rise to inconsistent cells, one of them is indicated with a circle; (b) choosing different step sizes in each basis yields a consistent EVQ.

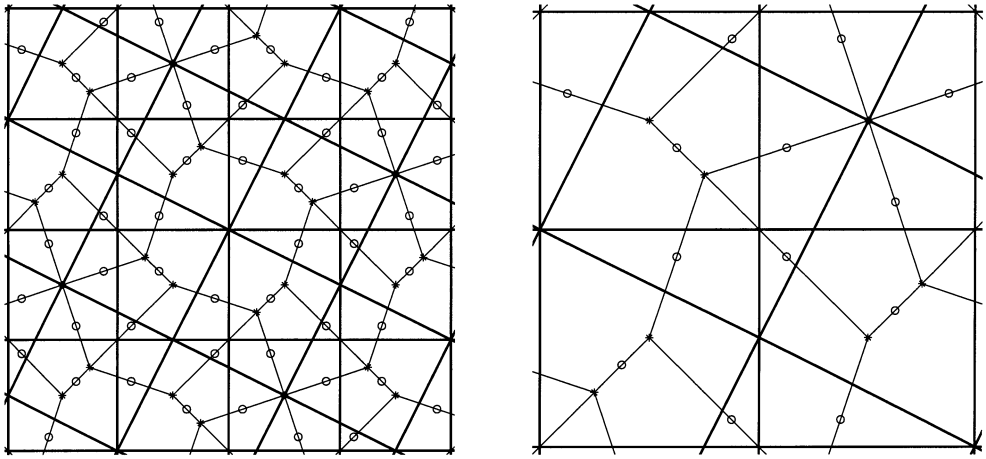

(a) (b)

Fig. 4. (a) Example of a linearly consistent quantizer EVQ, (b) (Zoom) four cells of Q^1. The reconstructions $\hat{\boldsymbol{x}}^j$, $j = 1, 2$ are represented by "$*$" and the final reconstruction $\hat{\boldsymbol{x}}$ is represented by "$\circ$."

on the angle between each of the bases. Fig. 4 shows a second example where consistency is achieved by creating a periodic structure.

III. Construction and Design of Quantizers With Periodic Structure

We call the type of quantizers shown in Fig. 3 "periodic quantizers" because the partition they generate has a periodic structure. We derive in detail how to design such quantizers in this section. The construction that we give in order to achieve periodicity is completely general. However, we provide designs only for redundant families (frames) of vectors with a certain constrained structure. More specifically, we give designs mostly for the case of having r orthogonal bases in $\mathbb{R}^2$. Some designs extensions for $\mathbb{R}^2$ are given in Section III-E where several examples are given, and extensions to higher dimensions are analyzed in Section III-D.

A. Definition and Construction of Periodic EVQs for $\mathbb{R}^2$

In order to facilitate the understanding, we first provide a detailed derivation of how to impose a periodic structure in EVQs in $\mathbb{R}^2$ for the case of redundancy $r = 2$. Then, we extend the idea to higher redundancies also in $\mathbb{R}^2$, and, finally, we explain how to obtain periodic structures in higher dimensions.

In designing an EVQ with a periodic structure, we will use the concept of sublattice.

Definition 9 [23]: A sublattice $\Lambda_s \in \Lambda$ of a given lattice Λ is a subset of the elements of Λ that is itself a lattice. A sublattice Λ_s is completely specified by an invertible integer matrix $\boldsymbol{B}_{\Lambda_s}$ that maps a basis of Λ into a basis of Λ_s, that is, $\boldsymbol{M}_{\Lambda_s} = \boldsymbol{B}_{\Lambda_s}\boldsymbol{M}_{\Lambda}$, where $\boldsymbol{M}_{\Lambda_s}$ and $\boldsymbol{M}_{\Lambda}$ are the generator matrices of Λ_s and Λ, respectively.

Given a real full rank lattice[2] Λ with generator matrix $\boldsymbol{M}_{\Lambda}$, we consider only full-rank sublattices Λ_s, that is, $\mathrm{rank}\,(\boldsymbol{M}_{\Lambda}) =$

[2] Λ is said to be a full-rank lattice if its generator matrix $\boldsymbol{M}_{\Lambda}$ is full rank.

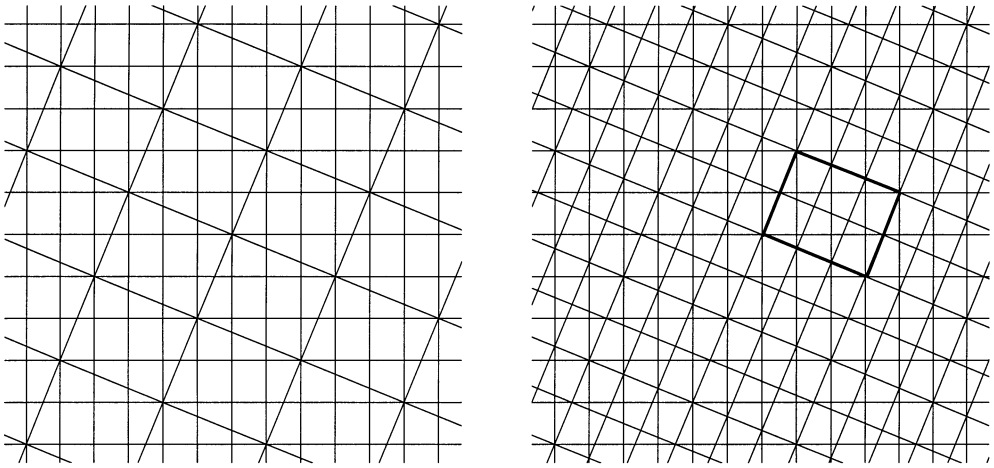

(a) (b)

Fig. 5. Example 1: (a) Sublattice structure (b) EVQ cells C^{EVQ}.

$\operatorname{rank}(\boldsymbol{M}_{\Lambda_s})$. Another important concept is that of the index of a sublattice Λ_s contained in a lattice Λ which is given by

$$|\Lambda/\Lambda_s| = \frac{\det(\boldsymbol{M}_{\Lambda_s})}{\det(\boldsymbol{M}_{\Lambda})} = \frac{\operatorname{Vol}(C_o^{\Lambda_s})}{\operatorname{Vol}(C_o^{\Lambda})} = |\det(\boldsymbol{B}_{\Lambda_s})|. \quad (11)$$

The index of a sublattice is the ratio of the volumes of the fundamental polytope associated with the sublattice Λ_s and the one associated with Λ. This is also equal to the number of lattice points of Λ contained in each cell defined by Λ_s. Notice that in the particular case of having an integer matrix $\boldsymbol{B}_{\Lambda_s}$ such that $|\det(\boldsymbol{B}_{\Lambda_s})| = 1$, Λ and Λ_s are the same lattice. This particular type of integer matrices satisfying this property are called *unimodular* matrices and by taking different unimodular matrices one can obtain different generator matrices for the same lattice.

We introduce the concept of geometrically scaled-similar sublattices from which we build periodic tesselations.

Definition 10: Given a real lattice Λ in $\mathbb{R}^2$ with generator matrix $\boldsymbol{M}_{\Lambda}$, a lattice Λ' is geometrically scaled-similar to Λ iff

$$\boldsymbol{M}_{\Lambda'} = \begin{pmatrix} c_1 & 0 \\ 0 & c_2 \end{pmatrix} \boldsymbol{U}\boldsymbol{M}_{\Lambda}\boldsymbol{R}, \quad (12)$$

where $\boldsymbol{R}$ is a 2×2 orthogonal matrix, that is, a rotation and/or a reflection in $\mathbb{R}^2$, $\boldsymbol{U}$ is a 2×2 unimodular integer matrix, and $c_1, c_2 \in \mathbb{R}_+$.

If Λ' is geometrically scaled-similar to Λ and is also a sublattice of Λ, then we denote it by $S\Lambda$. Note that this can only be true for specific values of c_1, c_2, and $\boldsymbol{R}$.

Thus, a geometrically scaled-similar sublattice $S\Lambda$ of a lattice Λ is obtained by simply rotating and/or reflecting the lattice Λ and then scaling each of the new axes. The matrix $\boldsymbol{U}$ allows us to choose different basis vectors for the sublattice $S\Lambda$. If $\det(\boldsymbol{R}) = +1$, then $\boldsymbol{R}$ is a pure rotation, and the scaling parameters c_1 and c_2 allow to control the magnitudes in each of the two vectors that define its basis. If $\det(\boldsymbol{R}) = -1$, then $\boldsymbol{R}$ contains or is a reflection. The possible orientations and values for c_1 and c_2 that determine a geometrically scaled-similar sublattice will be given in Section III-B. Notice that in the particular case of having $c_1 = c_2$, $S\Lambda$ would be a geometrically similar (or equivalent) sublattice of Λ, as defined by Conway *et al.* [24], [23]. We restrict $\boldsymbol{R}$ to be a pure rotation so that we can associate each rotation with a basis of a frame, as we explain next. Fig. 5(a) shows an example for a redundancy $r = 2$ of a geometrically scaled-similar sublattice of a rectangular lattice.

Without loss of generality, in the following we will construct geometrically scaled-similar sublattices of a canonical lattice Λ^1, where Λ^1 has generator matrix

$$\boldsymbol{M}_{\Lambda^1} = \begin{pmatrix} \Delta_1^1 & 0 \\ 0 & \Delta_2^1 \end{pmatrix} \quad (13)$$

that is, the generator vectors of Λ^1 are scaled versions of the canonical basis vectors $\boldsymbol{\varphi}_1^1 = [1, 0]^T$, $\boldsymbol{\varphi}_2^1 = [0, 1]^T$ ($\boldsymbol{F}^1 = \boldsymbol{I}_{2\times 2}$). We define the quantizer Q^1 as the quantizer with rectangular cells C^{Λ^1} whose vertices are given by the lattice Λ^1.

Notational Remark: In order to distinguish between the cells associated with a lattice Λ^j or a quantizer Q^j and the cells associated with a sublattice $S\Lambda^j \subset \Lambda^j$, we will use the following notation: a) C^{Λ^j} will denote the set of cells associated with Λ^j and Q^j, where we use now C^{Λ^j} instead of C^j in order to emphasize that these cells are associated with the lattice Λ^j; b) $C^{S\Lambda^j}$ will denote the set of cells associated with $S\Lambda^j$. The subscript will indicate in both cases a particular cell.

Definition 11 (Periodicity Property): An EVQ is said to be periodic if the partition of the space given by its quantizing cells satisfies the following two properties.

1) There exists a minimal periodic unit C_o^{EVQ} which is the union of a finite set of cells $\{\mathcal{P}_1, \ldots, \mathcal{P}_m\}$.
2) There exists a lattice Λ which determines this periodicity such that all the cells of the EVQ are given by $\{\mathcal{P}_1, \ldots, \mathcal{P}_k\} + \Lambda$, that is, copies of the minimal unit C_o^{EVQ} translated by the points of Λ.

Fig. 5(b) shows the unit cell C_o^{EVQ} with bold lines for a particular EVQ with redundancy $r = 2$. The periodicity structure is achieved by finding lattices whose intersection is not empty, which involves the concept of sublattice.

Fact 1: If Λ_s is a sublattice of Λ^1, the partition defined by the intersection of the cells C^{Λ^1} with the cells determined by Λ_s has a periodic structure (tesselation) with the minimal periodic unit given by $C^{\Lambda^1} \cap C_o^{\Lambda_s}$, where $C_o^{\Lambda_s}$ is the fundamental polytope associated with the sublattice Λ_s and the whole tesselation is obtained by translating the cells $C^{\Lambda^1} \cap C_o^{\Lambda_s}$ with the points of Λ_s.

Proof: See Appendix I.

This fact can be observed in Fig. 5(a) where in this case, the sublattice is a geometrically scaled-similar sublattice. In this work, we use Fact 1 for the particular case where the sublattices are geometrically scaled-similar.

Definition 12: Given a set of lattices Λ^j, $j = 1, \ldots, r$, the coincidence site lattice (CSL) Λ^{CSL} is the intersection lattice:

$$\Lambda^{\mathrm{CSL}} = \Lambda^1 \cap \Lambda^2 \cap \cdots \cap \Lambda^r \tag{14}$$

which is the finest common sublattice of all the lattices Λ^j, $j = 1, \ldots, r$.

In order to achieve periodicity, our goal is to construct a set of lattices $\Lambda^1, \Lambda^2, \ldots, \Lambda^r$ whose intersection is not empty. For this, it is sufficient to find a set of geometrically scaled-similar sublattices $S\Lambda^1, S\Lambda^2, \ldots, S\Lambda^r$ of the first lattice Λ^1. For notational convenience, we take $S\Lambda^1 = \Lambda^1$ and we will always take $\boldsymbol{U} = \boldsymbol{I}$ in (12) so that the basis vectors of the jth geometrically scaled-similar sublattice are orthogonal (because of the rotation matrix) and can be associated with the jth orthogonal basis of a tight frame. Each rectangular cell $C_i^{S\Lambda^j}$ defined by each sublattice $S\Lambda^j$ has sides with lengths $c_1^j\Delta_1^1$ and $c_2^j\Delta_2^1$. Since we have that $c_1^j, c_2^j \geq 1\ \forall j$, $\mathrm{Vol}\,(S\Lambda^j) = c_1^j c_2^j \mathrm{Vol}\,(\Lambda^1) \geq \mathrm{Vol}\,(\Lambda^1)$. Moreover, since the index of a sublattice is always an integer, we have that $c_1^j \times c_2^j \in \mathbb{Z}\ \forall j$.

Suppose we design jointly a lattice $\Lambda^1 = S\Lambda^1$ with generator matrix $\boldsymbol{M}_{\Lambda^1} = \mathrm{diag}\,[\Delta_1^1, \Delta_2^1]$ (choosing certain values for Δ_1^1, Δ_2^1), and $r-1$ different geometrically scaled-similar sublattices of Λ^1 denoted by $S\Lambda^2, S\Lambda^3, \ldots, S\Lambda^r$. Given a sublattice $S\Lambda^j$, we define a finer lattice $\Lambda^j \supset S\Lambda^j$ with generator matrix given by

$$\begin{aligned}
\boldsymbol{M}_{\Lambda^j} &= \begin{pmatrix} \frac{1}{d_1^j} & 0 \\ 0 & \frac{1}{d_2^j} \end{pmatrix} \boldsymbol{M}_{S\Lambda^j} \\
\boldsymbol{M}_{S\Lambda^j} &= \boldsymbol{B}_{S\Lambda^j} \begin{pmatrix} \Delta_1^1 & 0 \\ 0 & \Delta_2^1 \end{pmatrix} \\
\boldsymbol{B}_{S\Lambda^j} &= \begin{pmatrix} k_{11}^j & k_{12}^j \\ -k_{21}^j & k_{22}^j \end{pmatrix}
\end{aligned} \tag{15}$$

where $d_1^j, d_2^j, k_{11}^j, k_{12}^j, k_{21}^j, k_{22}^j \in \mathbb{Z}_+$, that is, are any positive integers.

As we show in Lemma 1 later, if we associate r quantizers $\{Q^j\}_{j=1}^r$, respectively, with the lattices $\{\Lambda^j\}_{j=1}^r$, this construction given above is sufficient in order to ensure that the intersection of all the lattices Λ^j, $j = 1, \ldots, r$ is not empty, and therefore, by group theory, the intersection is a lattice. Notice that if we consider only one lattice Λ^j together with the canonical lattice Λ^1, both constructed as described in (15), and we define corresponding quantizers Q^1 and Q^j, respectively associated with them, it follows from Fact 1 and because $\{d_1^j, d_2^j\}$ are positive integers, that the cells given by $C^{\Lambda^1} \cap C^{\Lambda^j}$ have a periodic structure, which is still determined by $C_o^{S\Lambda^j}$ (see Fig. 5(b)). Therefore, for $r = 2$, it is clear that periodicity holds.

Next, we show that the construction of $\Lambda^1, \ldots, \Lambda^r$ given above ensures that these lattices have a nonempty intersection, which actually implies a periodic structure[3] in the resulting EVQ.

Lemma 1: Given a set of lattices $\{\Lambda^j\}_{j=2}^{j=r}$, such that $\Lambda^j \supset S\Lambda^j$ and $S\Lambda^j$ is a sublattice of Λ^1 $j = 2, \ldots, r$, then the CSL contains as a sublattice, a lattice Λ^o that is an integer scaling of Λ^1, that is, $\boldsymbol{M}_{\Lambda^o} = D\boldsymbol{M}_{\Lambda^1}$, where $D \in \mathbb{Z}$.

Proof: See Appendix II. The importance of calculating the CSL Λ^{CSL} comes from the fact that its fundamental cell C_o^{CSL} is the unit cell that is repeated in the periodic structure of the resulting EVQ, as shown in the following lemma.

Lemma 2: Given r quantizers Q^j, $j = 1, \ldots, r$, associated with the lattices Λ^j, $j = 1, \ldots, r$, the partition of EVQ cells has a periodic structure, with the unit cell that is repeated periodically being C_o^{CSL}, the fundamental polytope of the CSL Λ^{CSL}.

Proof: See Appendix III.

Notice that any other lattice that is also a sublattice (although coarser than the CSL) of all the lattices Λ^j, $j = 1, \ldots, r$ determines also a unit cell that is repeated periodically but this unit cell will be larger than C_o^{CSL}. For instance, the fundamental polytope of the rectangular lattice Λ^o described in Lemma 1, will be also repeated periodically but $\mathrm{Vol}\,(\Lambda^o) \geq \mathrm{Vol}\,(\Lambda^{\mathrm{CSL}})$.

Next, we show how simple it is to calculate the generator matrix of the CSL Λ^{CSL} for any dimension N. For this, it is necessary to first review the following concept for N-dimensional lattices.

Definition 13: Given r N-dimensional lattices Λ^j, $j = 1, \ldots, r$ in $\mathbb{R}^N$ satisfying the property that $\exists$ an N-dimensional lattice Λ^F for which $\Lambda^j \subset \Lambda^F$, $j = 1, \ldots, r$, we define the (N-dimensional) sum lattice $\Lambda^\Sigma = \Lambda^1 + \Lambda^2 + \cdots \Lambda^r$ as follows [26]:

$$\Lambda^\Sigma = \left\{\boldsymbol{y} \in \mathbb{R}^N \colon \boldsymbol{y} = \boldsymbol{x}\boldsymbol{A}, \boldsymbol{x} \in \mathbb{Z}^{rN}\right\},$$
$$\text{where } \boldsymbol{A} = \begin{pmatrix} \boldsymbol{M}_{\Lambda^1} \\ \boldsymbol{M}_{\Lambda^2} \\ \vdots \\ \boldsymbol{M}_{\Lambda^r} \end{pmatrix}. \tag{16}$$

Remark: The lattice Λ^Σ is the lattice generated by all the basis vectors of all the lattices Λ^j, $j = 1, \ldots, r$ in $\mathbb{R}^N$ (not simply the union of the lattice points). The matrix $\boldsymbol{A}$ defined above can be reduced to obtain the actual $(N \times N)$ generator matrix $\boldsymbol{M}_{\Lambda^\Sigma}$ using the so-called Hermite normal form (HNF) reduction algorithm [26].

Definition 14: The dual lattice Λ^* of a lattice Λ in $\mathbb{R}^N$ is defined as follows [23]:

$$\Lambda^* = \left\{\boldsymbol{v} \in \mathbb{R}^N \colon \langle \boldsymbol{v}, \boldsymbol{w} \rangle \in \mathbb{Z} \quad \forall \boldsymbol{w} \in \Lambda\right\}. \tag{17}$$

[3]Notice that a periodic tesselation may be obtained also using other methods which are not based on intersecting lattices, that is, forcing the intersection of the lattices $\Lambda^1, \ldots, \Lambda^r$ is just one (purely geometrical) way to obtain a periodic tesselation, but one could also build a periodic tesselation in other ways.

The generator matrix of Λ^* is given by $\boldsymbol{M}_{\Lambda^*} = ((\boldsymbol{M}_\Lambda)^{-1})^T$, and we have also that $(\Lambda^*)^* = \Lambda$ [23].

It is important to note that the sum of two lattices Λ^1 and Λ^2 is not necessarily a lattice; for instance, taking $\Lambda^1 = \mathbb{Z}$ and $\Lambda^2 = \sqrt{2}\mathbb{Z}$, then their sum is not a lattice because the sum is not a discrete subgroup of $\mathbb{R}$. It can be shown [30], [31] that if Λ^1 and Λ^2 are contained in a certain full-rank lattice Λ^F, then $\Lambda^1 + \Lambda^2$ is a full-rank lattice.

Based on the previous definitions, the following important theorem from lattice theory allows us to calculate the intersection lattice Λ^{CSL} of a set of lattices $\Lambda^1, \ldots, \Lambda^r$ [27], [28].

Theorem 1: Given r lattices Λ^j, $j = 1, \ldots, r$, the following holds:

$$\begin{aligned} &\left(\Lambda^1\right)^* + \cdots + (\Lambda^r)^* = \left(\Lambda^1 \cap \cdots \cap \Lambda^r\right)^* \\ \Longleftrightarrow\ &\left(\left(\Lambda^1\right)^* + \cdots + (\Lambda^r)^*\right)^* = \Lambda^1 \cap \cdots \cap \Lambda^r = \Lambda^{\mathrm{CSL}}. \end{aligned} \tag{18}$$

Notice that using Lemma 1 the construction of the lattices $\Lambda^1, \ldots, \Lambda^r$ we have presented here ensures that Λ^{CSL} always exist and is a full-rank lattice, implying a periodic structure in the EVQ. The necessary and sufficient condition for $\Lambda^1 \cap \Lambda^2$ to exist and be a full-rank lattice is that the matrix $(M_{\Lambda^1})^{-1} M_{\Lambda^2}$ be a matrix of rational numbers. This condition is implicitly used in order to prove Lemma 1. In the same way, our construction also ensures that $(\Lambda^1)^* + (\Lambda^2)^*$ always exists and is a full-rank lattice. The lattice $\Lambda^1 \cap \Lambda^2$ is the finest lattice which is a sublattice of Λ^1 and Λ^2, while the sum $\Lambda^1 + \Lambda^2$ is the coarsest lattice which contains both Λ^1 and Λ^2 as sublattices.

B. Design and Parameterization for $\mathbb{R}^2$

Let Λ^1 be a rectangular lattice in $\mathbb{R}^2$ with generator matrix $\boldsymbol{M}_{\Lambda^1} = \mathrm{diag}\,[\Delta_1^1, \Delta_2^1]$, which defines a quantizer Q^1. In $\mathbb{R}^2$, it is easy to parameterize all the geometrically scaled-similar sublattices of Λ^1 in terms of the possible *scaling factors* and *rotation* matrices as in (12). This parameterization can be used in order to build a periodic EVQ in $\mathbb{R}^2$ for any redundancy r.

Fact 2: All geometrically scaled-similar sublattices $S\Lambda$ of Λ^1 with $\boldsymbol{M}_{\Lambda^1} = \mathrm{diag}\,[\Delta_1^1, Delta_2^1]$ have generator matrices that can be characterized geometrically in the following way:

$$\boldsymbol{M}_{S\Lambda} = \begin{pmatrix} c_1\Delta_1^1 & 0 \\ 0 & c_2\beta\Delta_1^1 \end{pmatrix} \begin{pmatrix} \cos(\theta) & \sin(\theta) \\ -\sin(\theta) & \cos(\theta) \end{pmatrix} \tag{19}$$

where

$$\beta = \frac{\Delta_2^1}{\Delta_1^1} = \sqrt{\frac{k_{11}k_{21}}{k_{12}k_{22}}}, \quad \tan(\theta) = \sqrt{\frac{k_{12}k_{21}}{k_{11}k_{22}}} = \frac{k_{12}}{k_{11}}\,\beta$$
$$c_1 = \frac{k_{11}}{\cos(\theta)}, \quad c_2 = \frac{k_{22}}{\cos(\theta)}$$

and $k_{11}, k_{12}, k_{21}, k_{22}$ are any positive integers and $0 < \theta < \frac{\pi}{2}$.

Proof: See Appendix IV.

The angle θ is restricted to the interval $]0, \frac{\pi}{2}[$ to avoid duplicity. That is, given a valid angle $\theta \in]0, \frac{\pi}{2}[$, the angles $\theta + i\frac{\pi}{2}$, $i = 1, 2, 3$ generate the same sublattice $S\Lambda$ because the basis vectors will be inverted versions of the ones corresponding to $\theta \in]0, \frac{\pi}{2}[$.

The generator matrix of lattice Λ^j, as given in (15), and step sizes $\{\Delta_1^j, \Delta_2^j\}$ associated with the scalar quantizers $\{SQ_1^j, SQ_2^j\}$ can be parameterized by

$$M_{\Lambda^j} = \begin{pmatrix} \frac{k_{11}^j}{d_1^j} & \frac{k_{12}^j}{d_1^j}\,\beta \\ \frac{-k_{21}^j}{d_2^j} & \frac{k_{22}^j}{d_2^j}\,\beta \end{pmatrix} \Delta_1^1$$
$$\Delta_1^j = \frac{\Delta_1^1}{d_1^j}\sqrt{\frac{k_{11}^j}{k_{22}^j}\left(k_{11}^j k_{22}^j + k_{12}^j k_{21}^j\right)}$$
$$\Delta_2^j = \frac{\Delta_1^1}{d_2^j}\sqrt{\frac{k_{21}^j}{k_{12}^j}\left(k_{11}^j k_{22}^j + k_{12}^j k_{21}^j\right)}. \tag{20}$$

A few comments are in order.

1) Only those angles θ such that $\tan(\theta) = \sqrt{m_1/m_2}$, $m_1, m_2 \in \mathbb{Z}_+$, lead to geometrically scaled-similar sublattices.

2) For a given fixed angle θ there is more than one solution for β, c_1, and c_2.

3) The product $c_1c_2 = |\Lambda/S\Lambda| \in \mathbb{Z}_+$, as it should be, because

$$\begin{aligned} c_1c_2 &= k_{11}k_{22}\left(\frac{1}{\cos(\theta)}\right) = k_{11}k_{22}\left(1 + (\tan(\theta))^2\right) \\ &= k_{11}k_{22} + k_{12}k_{21} = \det(\boldsymbol{B}_{S\Lambda}) \in \mathbb{Z}_+. \end{aligned} \tag{21}$$

4) If we consider the particular case of having $c_1 = c_2 = c$ and $\beta = 1$, that is, geometrically similar sublattices of the cubic real lattice $\mathbb{Z}^2_{\Delta_1^1}$, then, the possible solutions are[4]

$$\tan(\theta) = \frac{b}{a}, \quad c = \sqrt{a^2 + b^2}, \quad \cos(\theta) = \frac{a}{\sqrt{a^2 + b^2}}$$
$$\sin(\theta) = \frac{b}{\sqrt{a^2 + b^2}}, \qquad a, b \in \mathbb{Z}_+ \tag{22}$$

which agrees with [24].

Although periodicity in the structure holds for any two positive integers d_1^j and d_2^j, in practice, each pair (d_1^j, d_2^j) is constrained to some values to provide good quantization performance. Therefore, it is desirable not to have a cell of a quantizer Q^{j_1} completely contained within a cell of another quantizer Q^{j_2}. Ideally, adding successive quantizers Q^j will lead to reductions in the size of the EVQ cells (and, therefore, in distortion). Appendix V describes in detail a simple geometric criterion that can be used to address this issue. There is no unique way for the order in which one can choose the different parameters. One possible way is by fixing the angle θ first, that is, choosing a value for $\sqrt{(k_{12}k_{21})/(k_{11}k_{22})}$, then searching within all the 4-tuples of integers resulting in that value, and for each of these 4-tuples we obtain certain values for the step sizes using (20).

C. Examples of Periodic EVQs in $\mathbb{R}^2$

We present in this section several design examples for the 2-D case.

Example 1: Let us choose an angle θ such that $\tan(\theta) = \sqrt{2 \times 3}$. A possible choice for the constant integers is

[4]Notice that we are restricting the angle θ to be $0 < \theta < \frac{\pi}{2}$.

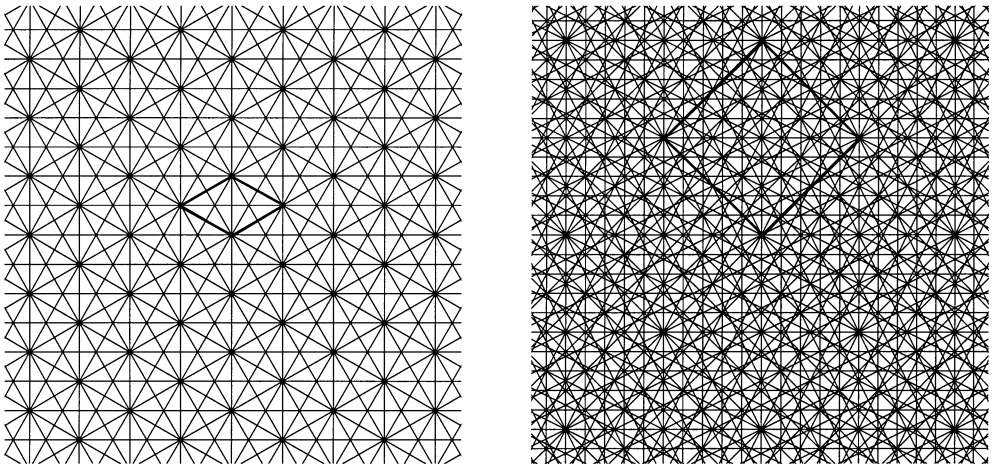

(a) (b)

Fig. 6. (a) Example for $r = 3$: Structure of the EVQ and unit cell of the structure. (b) Example for $r = 4$: Structure of the EVQ and unit cell. Notice that in (b) due to the symmetry that exists within C_o^{CSL}, the effective number of different EVQ cells is basically $1/8$ of the total number of cells within this unit cell.

$k_{11}^2 = k_{22}^2 = 1$, $k_{12}^2 = 2$, and $k_{21}^2 = 3$. If we choose $d_1^2 = 2$ and $d_2^2 = 3$, the resulting quantizer Q^2 is given by

$$\beta = \sqrt{\frac{3}{2}}, \quad \Delta_1^2 = \sqrt{\frac{3}{2}}\,\Delta_1^1$$
$$\Delta_1^2 = \frac{1}{\cos(\theta)}\,\Delta_1^1, \quad \Delta_2^2 = \frac{1}{\cos(\theta)}\sqrt{\frac{3}{2}}\,\Delta_1^1. \tag{23}$$

The corresponding EVQ cells are shown in Fig. 5(b).

Example 2: A good example for $r = 3$ is obtained by using the following tight frame and step sizes:

$$\boldsymbol{F} = \begin{pmatrix} 1 & 0 \\ 0 & 1 \\ \cos\left(\frac{\pi}{6}\right) & \sin\left(\frac{\pi}{6}\right) \\ -\sin\left(\frac{\pi}{6}\right) & \cos\left(\frac{\pi}{6}\right) \\ \cos\left(\frac{\pi}{3}\right) & \sin\left(\frac{\pi}{3}\right) \\ -\sin\left(\frac{\pi}{3}\right) & \cos\left(\frac{\pi}{3}\right) \end{pmatrix}$$
$$\beta = \frac{1}{\sqrt{3}}, \quad \Delta_2^1 = \beta\Delta_1^1 = \frac{1}{\sqrt{3}}\,\Delta_1^1$$
$$\Delta_1^2 = \frac{1}{2}\left(\frac{1}{\cos\left(\frac{\pi}{6}\right)}\right)\Delta_1^1, \quad \Delta_2^2 = \frac{1}{2}\left(\frac{3}{\cos\left(\frac{\pi}{6}\right)}\right)\left(\frac{1}{\sqrt{3}}\right)\Delta_1^1$$
$$\Delta_1^3 = \frac{1}{2}\left(\frac{1}{\cos\left(\frac{\pi}{3}\right)}\right)\Delta_1^1, \quad \Delta_2^3 = \frac{1}{2}\left(\frac{1}{\cos\left(\frac{\pi}{3}\right)}\right)\left(\frac{1}{\sqrt{3}}\right)\Delta_1^1. \tag{24}$$

Notice that in this example, $d_1^2 = d_2^2 = d_1^3 = d_2^3 = 2$. Fig. 6(a) shows the unit cell that is repeated periodically and the resulting EVQ cells. In this example, we have that

$$\boldsymbol{M}_{\Lambda^{CSL}} = \begin{pmatrix} 1 & 1 \\ -1 & 1 \end{pmatrix}\boldsymbol{M}_{\Lambda^1} = \begin{pmatrix} 1 & 1 \\ -1 & 1 \end{pmatrix}\begin{pmatrix} 1 & 0 \\ 0 & \frac{1}{\sqrt{3}} \end{pmatrix}\Delta_1^1$$
$$= \begin{pmatrix} 1 & \frac{1}{\sqrt{3}} \\ -1 & \frac{1}{\sqrt{3}} \end{pmatrix}\Delta_1^1$$
$$\boldsymbol{M}_{\Lambda^o} = \begin{pmatrix} 2 & 0 \\ 0 & 2 \end{pmatrix}\boldsymbol{M}_{\Lambda^1} = 2\begin{pmatrix} 1 & 0 \\ 0 & \frac{1}{\sqrt{3}} \end{pmatrix}\Delta_1^1. \tag{25}$$

Example 3: An example for $r = 4$ can be obtained by using the following tight frame and step sizes:

$$\boldsymbol{F} = \begin{pmatrix} 1 & 0 \\ 0 & 1 \\ \frac{1}{\sqrt{2}} & \frac{1}{\sqrt{2}} \\ \frac{-1}{\sqrt{2}} & \frac{1}{\sqrt{2}} \\ \frac{1}{\sqrt{5}} & \frac{2}{\sqrt{5}} \\ \frac{-2}{\sqrt{5}} & \frac{1}{\sqrt{5}} \\ \frac{2}{\sqrt{5}} & \frac{1}{\sqrt{5}} \\ \frac{-1}{\sqrt{5}} & \frac{2}{\sqrt{5}} \end{pmatrix} \quad \begin{aligned} &\beta = 1, \quad \Delta_2^1 = \beta\Delta_1^1 = \Delta_1^1 \\ &\Delta_1^2 = \sqrt{2}\Delta_1^1, \quad \Delta_2^2 = \sqrt{2}\Delta_1^1 \\ &\Delta_1^3 = \tfrac{\sqrt{5}}{2}\,\Delta_1^1, \quad \Delta_2^3 = \tfrac{\sqrt{5}}{2}\,\Delta_1^1 \\ &\Delta_1^4 = \tfrac{\sqrt{5}}{2}\,\Delta_1^1, \quad \Delta_2^4 = \tfrac{\sqrt{5}}{2}\,\Delta_1^1 \\ &\Delta_1^5 = \tfrac{\sqrt{5}}{2}\,\Delta_1^1, \quad \Delta_2^5 = \tfrac{\sqrt{5}}{2}\,\Delta_1^1 \\ &\Delta_1^6 = \tfrac{\sqrt{5}}{2}\,\Delta_1^1, \quad \Delta_2^6 = \tfrac{\sqrt{5}}{2}\,\Delta_1^1. \end{aligned} \tag{26}$$

Fig. 6(b) shows the unit cell that is repeated periodically and the resulting EVQ cells. In this example, we have that

$$\boldsymbol{M}_{\Lambda^{CSL}} = \begin{pmatrix} -5 & 5 \\ 5 & 5 \end{pmatrix}\boldsymbol{M}_{\Lambda^1} = \begin{pmatrix} -5 & 5 \\ 5 & 5 \end{pmatrix}\Delta_1^1$$
$$\boldsymbol{M}_{\Lambda^o} = \begin{pmatrix} 10 & 0 \\ 0 & 10 \end{pmatrix}\boldsymbol{M}_{\Lambda^1} = \begin{pmatrix} 10 & 0 \\ 0 & 10 \end{pmatrix}\Delta_1^1. \tag{27}$$

Notice in these two examples how we have chosen the step sizes of the different quantizers $\{Q^j\}_{j=1}^r$ trying to satisfy as much as possible the constraints mentioned in Section III-B (refinement between different quantizers).

D. Design of Periodic EVQs in Higher Dimensions

We now analyze the extension to higher dimensions for the case where $\boldsymbol{M}_{\Lambda^1} = \boldsymbol{I}\Delta_1^1$, that is, if the dimension is N, then $\Delta_1^1 = \Delta_2^1 = \cdots = \Delta_N^1$. Since Λ^1 is a cubic lattice, a geometrically scaled similar sublattice $S\Lambda$ has to be also cubic and thus its generator matrix has to be $\boldsymbol{M}_{S\Lambda} = \boldsymbol{B}_{S\Lambda}\boldsymbol{M}_{\Lambda^1} = \boldsymbol{B}_{S\Lambda}\Delta_1^1$, where the integer matrix $\boldsymbol{B}_{S\Lambda}$ satisfies the orthogonality property

$$\boldsymbol{B}_{S\Lambda}^T\boldsymbol{B}_{S\Lambda} = \begin{pmatrix} b_1 & 0 & \cdots & 0 \\ 0 & b_2 & \cdots & 0 \\ & & \ddots & \vdots \\ 0 & \cdots & & b_N \end{pmatrix}, \qquad b_1, b_2, \ldots, b_N \in \mathbb{Z}_+. \tag{28}$$

If $S\Lambda^j$ is the jth sublattice, we construct the jth lattice Λ^j as we have done before for $N = 2$, that is, dividing by integers $\{d_i^j\}_{i=1}^N$ and the associated orthogonal matrix $\boldsymbol{F}^j$ and step sizes $\{\Delta_i^j\}_{i=1}^N$ will be given by

$$\boldsymbol{F}^j = \begin{pmatrix} \frac{1}{\sqrt{b_1^j}} & 0 & \cdots & 0 \\ 0 & \frac{1}{\sqrt{b_2^j}} & \cdots & 0 \\ 0 & \cdots & \ddots & \vdots \\ 0 & 0 & \cdots & \frac{1}{\sqrt{b_N^j}} \end{pmatrix} \boldsymbol{B}_{S\Lambda^j}$$

$$\Delta_i^j = \frac{\sqrt{b_i^j}}{d_i^j}\,\Delta_1^1, \qquad d_i^j \in \mathbb{Z}_+ \tag{29}$$

and all the results regarding periodicity in the structure of the final EVQ and the CSL Λ^{CSL} apply also here.

Since the matrix $\boldsymbol{M}_{S\Lambda}$ is proportional to $\boldsymbol{B}_{S\Lambda}$ by Δ_1^1, let us focus on the problem of finding integer matrices $\boldsymbol{B}_{S\Lambda}$ satisfying the properties mentioned above, thus, looking at geometrically similar sublattices of $\mathbb{Z}^N$. Clearly, we can construct matrices $\boldsymbol{B}_{S\Lambda}$ in the following way:

$$\boldsymbol{B}_{S\Lambda} = \begin{pmatrix} a_1 & 0 & \cdots & 0 \\ 0 & a_2 & \cdots & 0 \\ 0 & \cdots & \ddots & \vdots \\ 0 & 0 & \cdots & a_N \end{pmatrix} \boldsymbol{H}_{S\Lambda}, \quad a_1, \ldots, a_N \in \mathbb{Z}$$

$$\boldsymbol{H}_{S\Lambda}^T \boldsymbol{H}_{S\Lambda} = \boldsymbol{H}_{S\Lambda} \boldsymbol{H}_{S\Lambda}^T = m\boldsymbol{I}, \qquad m \in \mathbb{Z}_+. \tag{30}$$

The problem of finding matrices $\boldsymbol{H}_{S\Lambda}$ satisfying the above property has been studied extensively [29], [32] and the algebraic theory of orthogonal designs allows to find general constructions of orthogonal matrices with indeterminate entries.

Notice that the matrices $\boldsymbol{H}_{S\Lambda}$ actually generate geometrically similar or equivalent sublattices with index $K = m^{N/2}$, $m \in \mathbb{Z}_+$. Explicit constructions in higher dimensions have been provided by Sloane and Beferull-Lozano and can be found in [22]. More specifically, constructions are given for dimensions $N = 3, 6, 12, 24, 2^k$, $k \geq 2$. For illustration purposes, we present here a simple example for $N = 4$. Details about the tesselation of the space that is generated are also given in [22].

Example 4:

$$\boldsymbol{M}_{\Lambda^1} = \begin{pmatrix} 2 & 0 & 0 & 0 \\ 0 & 2 & 0 & 0 \\ 0 & 0 & 2 & 0 \\ 0 & 0 & 0 & 2 \end{pmatrix} \Delta_1^1$$

$$\boldsymbol{M}_{\Lambda^2} = \begin{pmatrix} +1 & +1 & +1 & +1 \\ +1 & -1 & +1 & -1 \\ +1 & -1 & -1 & +1 \\ +1 & +1 & -1 & -1 \end{pmatrix} \Delta_1^1$$

$$\boldsymbol{M}_{\Lambda^3} = \begin{pmatrix} -1 & +1 & +1 & +1 \\ -1 & -1 & +1 & -1 \\ -1 & -1 & -1 & +1 \\ -1 & +1 & -1 & -1 \end{pmatrix} \Delta_1^1. \tag{31}$$

The intersection of these three lattices, that is, the CSL, can be easily calculated and is given by

$$\boldsymbol{M}_{\Lambda^{\mathrm{CSL}}} = \begin{pmatrix} 4 & 0 & 0 & 0 \\ 2 & 2 & 0 & 0 \\ 2 & 0 & 2 & 0 \\ 2 & 0 & 0 & 2 \end{pmatrix} \tag{32}$$

which is a version of the well-known lattice D_4 (best known lattice quantizer in four dimensions) on the scale at which its minimal squared norm is 8.

E. Design of Periodic EVQs for Other Redundant Families

It is also possible to construct periodic quantizers using families (frames) of vectors with integer redundancy r but which do not consist of a set of orthogonal bases. In this subsection, we show examples which are based on hexagonal lattices A_2 in $\mathbb{R}^2$, and sublattices which are geometrically similar ($c_1 = c_2 = c$) to hexagonal lattices.

Conway and Sloane [24] have parameterized all the possible sublattices which are geometrically similar to the hexagonal lattice $\Lambda^1 = A_2$, whose generator matrix is given by

$$\boldsymbol{M}_{\Lambda^1} = \begin{pmatrix} 1 & 0 \\ \frac{-1}{2} & \frac{\sqrt{3}}{2} \end{pmatrix} \Delta. \tag{33}$$

Notice that if we want to associate this lattice with a basis of a frame ($\boldsymbol{F}^1$), the vectors of this basis have to be orthogonal to the basis vectors of the lattice. Moreover, the step sizes associated with the vectors that compose $\boldsymbol{F}^1$ have to be calculated so that the lines in $\mathbb{R}^2$ intersect exactly to generate M_{Λ^1}. It is trivial to show by simple trigonometry that $\boldsymbol{F}^1$ and the associated step sizes are

$$\boldsymbol{F}^1 = \begin{pmatrix} 0 & 1 \\ \frac{\sqrt{3}}{2} & \frac{1}{2} \end{pmatrix} \qquad \Delta_1^1 = \Delta_2^1 = \frac{\sqrt{3}}{2}\Delta. \tag{34}$$

It is shown in [24] that a sublattice $S\Lambda$, which is geometrically similar to Λ^1, is generated by (using complex notation) $\boldsymbol{u} = a + b\omega$ and $\boldsymbol{v} = \omega(a + b\omega)$, where $\omega = -1/2 + i\sqrt{3}/2$, a, $b \in \mathbb{Z}$, and the index $|S\Lambda/\Lambda^1|$ of the corresponding sublattice is $|S\Lambda/\Lambda^1| = a^2 - ab + b^2$. Translating this to matrix notation, we have that the possible generator matrices for $S\Lambda$ are given by

$$\boldsymbol{M}_{S\Lambda} = \begin{pmatrix} \left(a - \frac{b}{2}\right) & \frac{\sqrt{3}}{2}\,b \\ -\frac{a+b}{2} & \frac{\sqrt{3}}{2}\,(a-b) \end{pmatrix} \Delta. \tag{35}$$

Notice also that M_{Λ^1} and $M_{S\Lambda}$ are related as follows:

$$\boldsymbol{M}_{S\Lambda} = \boldsymbol{M}_{\Lambda^1} \begin{pmatrix} \left(a - \frac{b}{2}\right) & \frac{\sqrt{3}}{2}\,b \\ -\frac{\sqrt{3}}{2}\,b & \left(a - \frac{b}{2}\right) \end{pmatrix} = \begin{pmatrix} a & b \\ -b & a-b \end{pmatrix} \boldsymbol{M}_{\Lambda^1} \tag{36}$$

which corresponds to a rotation of an angle θ such that $\tan(\theta) = \frac{\sqrt{3}b}{2a-b}$ and a scaling of $\sqrt{a^2 - ab + b^2}$. Using this approach, we can design again frames and PSQs such that a periodic EVQ is generated. Figs. 7 and 8 show examples of periodic EVQs for redundancies $r = 2$ and $r = 3$, respectively.

It is also possible to construct periodic EVQs for higher dimensions using redundant families which are not comprised of orthogonal bases, by means of other types of lattices such as

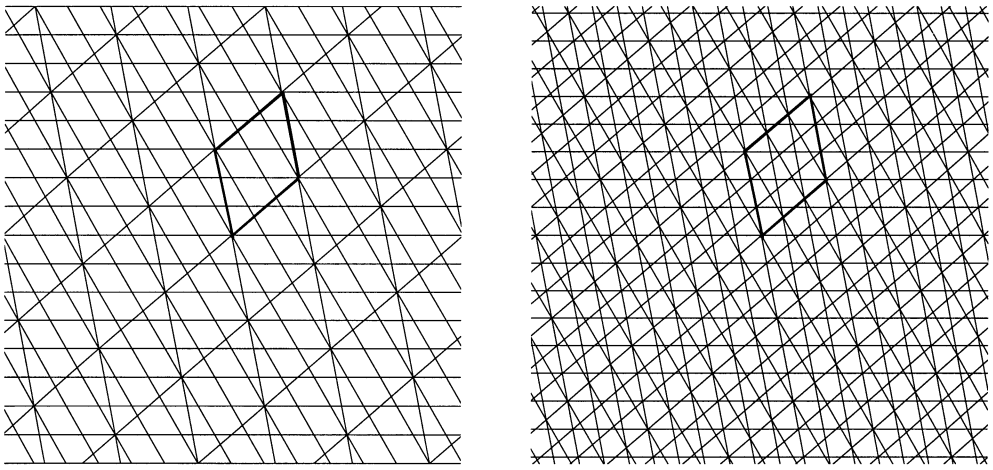

(a) (b)

Fig. 7. Example for $r = 2$. (a) Structure of the sublattice $S\Lambda$ with $a = 1$, $b = 3$. (b) Structure of the EVQ and unit cell.

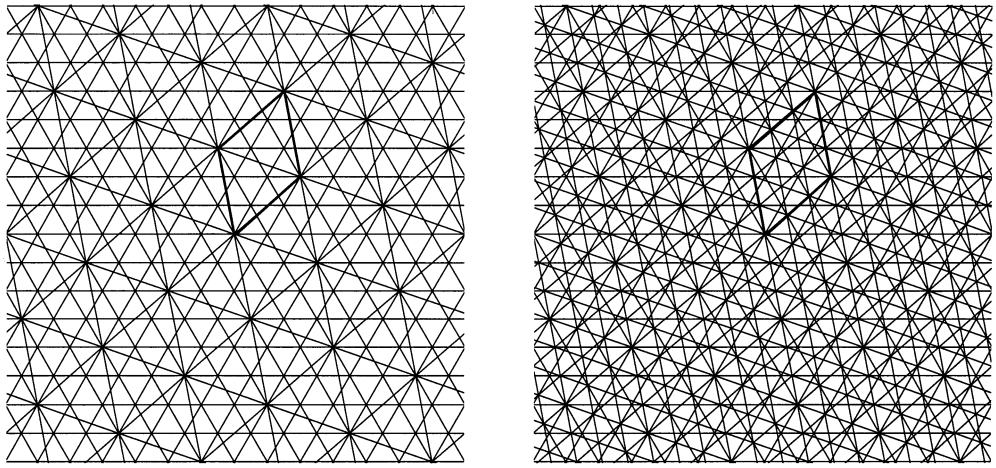

(a) (b)

Fig. 8. Example for $r = 3$. (a) Structure of the sublattice $S\Lambda$ with $a = 1$, $b = 3$. (b) Structure of the EVQ and unit cell.

those studied in [24] and [33], but these designs are not considered in this paper. Several examples of these other different constructions can also be found in [22].

IV. Consistent Reconstruction in Periodic Quantizers

In this section, we analyze how to achieve consistency in periodic quantizers under simple reconstruction algorithms (e.g., linear or lookup table).

A. Consistency Under Linear Reconstruction Using the Minimal Dual Frame

Although the results presented in this section hold for any type of frame and any type of linear reconstruction algorithm, the proofs of these results are much clearer and much more intuitive for the case of linear reconstruction using the minimal dual frame and for tight frames composed of a set of r orthogonal bases. We show in Theorem 2 that, given a frame, a necessary condition to have consistency under linear reconstruction is that the scalar quantizers acting on the coefficients are such that the resulting EVQ has a periodic structure. This result follows basically from the fact that when there is no periodicity in the partition defined by an EVQ, the vertices of any two lattices Λ^{j_1} and Λ^{j_2} $(j_1 \neq j_2)$ can have arbitrary relative positions, at least in one of the components, which makes it always possible to find linearly inconsistent cells. On the contrary, when there is periodicity, there is only a finite number of relative positions (see Fig. 4) and linear consistency is not precluded.

The proof of this result is exactly the same conceptually for any value of the redundancy r and for any dimension N because the crucial point is just the periodicity in the structure regardless of the underlying frame that is used. Since for higher dimensions N and higher redundancies r the proof becomes much more tedious without adding anything new conceptually, we reduce the proof to the $r = 2$ and $N = 2$ case. However, for completeness, examples will be shown where linear consistency is satisfied for $r > 2$ in $\mathbb{R}^2$.

We need the following lemma.

Lemma 3: Let Λ^1 be a rectangular lattice with

$$\boldsymbol{M}_{\Lambda^1} = \mathrm{diag}[\Delta_1^1, \Delta_2^1]$$

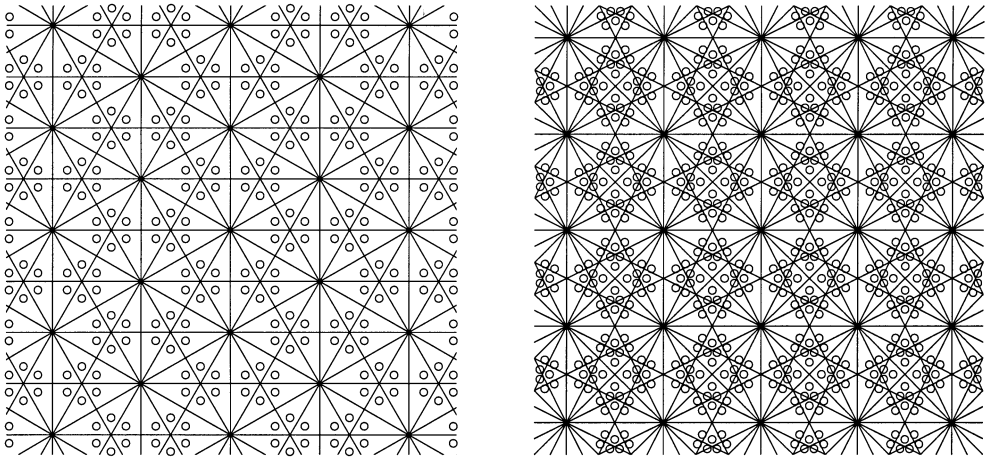

(a) (b)

Fig. 9. Examples of Linearly Consistent Quantizers for (a) $r = 3$ and (b) for $r = 4$. Minimal dual frame is used for the linear reconstruction.

and Λ^2 another (generic) lattice whose generator matrix is parameterized as

$$\boldsymbol{M}_{\Lambda^2} = \begin{pmatrix} \Delta_1^2 & 0 \\ 0 & \Delta_2^2 \end{pmatrix} \begin{pmatrix} \cos(\theta) & \sin(\theta) \\ -\sin(\theta) & \cos(\theta) \end{pmatrix}.$$

$$\text{where } \Delta_1^2,\ \Delta_2^2 \in \mathbb{R}_+,\ \theta \in \left]0,\ \frac{\pi}{2}\right[. \quad (37)$$

Then, the following equations:

$$\Delta_1^2 \cos(\theta) - \Delta_2^2 \sin(\theta) = q_1 \Delta_1^1 \quad (38)$$

$$\Delta_1^2 \cos(\theta) + \Delta_2^2 \sin(\theta) = q_2 \Delta_1^1 \quad (39)$$

$$\Delta_1^2 \sin(\theta) + \Delta_2^2 \cos(\theta) = q_3 \Delta_2^1 \quad (40)$$

$$\Delta_1^2 \sin(\theta) - \Delta_2^2 \cos(\theta) = q_4 \Delta_2^1 \quad (41)$$

$$\text{where } q_1,\ q_2,\ q_3,\ q_4 \in \mathbb{Q} \text{ (rational numbers)}$$

are all satisfied iff $\boldsymbol{M}_{\Lambda^2} = \text{diag}\,[1/d_1^2,\ 1/d_2^2]\boldsymbol{M}_{S\Lambda^2}$ where $S\Lambda^2$ is a sublattice of Λ^1, that is, $\boldsymbol{M}_{S\Lambda^2}$ is given as in (19), and $d_1^2,\ d_2^2 \in \mathbb{Z}_+$.

Proof: See Appendix VI.

The consequence of this lemma is that, when Λ^2 meets the conditions of the lemma, the vertices belonging to Λ^2, which can also be written as

$$\{\boldsymbol{\omega}_i\} = \left\{k_1\left(\Delta_1^2\boldsymbol{\varphi}_1^2 + \Delta_2^2\boldsymbol{\varphi}_2^2\right) + k_2\left(\Delta_1^2\boldsymbol{\varphi}_1^2 - \Delta_2^2\boldsymbol{\varphi}_2^2\right),\right.$$

$$\left. k_1,\ k_2 \in \mathbb{Z}\right\} \quad (42)$$

have only a finite number of different (relative) positions within the cells C^{Λ^1} of the quantizer Q^1 (see, for example, Fig. 5(b)). In Theorem 2, we use this fact so that if any of the previous four equations (38)–(41) is not satisfied, we can always find vertices where at least one component can have any arbitrary position within a cell of the quantizer Q^1, and this allows us to find (linearly) inconsistent cells.

Theorem 2: If the EVQ is a nonperiodic quantizer in $\mathbb{R}^2$, then it is always possible to find a linearly inconsistent cell.

Proof: See Appendix VII.

Thus, periodicity in an EVQ is a necessary condition to achieve consistency under linear reconstruction. Notice that in a periodic EVQ there are only finitely many distinct EVQ cells. Checking whether linear consistency is satisfied, we only need to check on the distinct EVQ cells, which are actually the EVQ cells inside the fundamental polytope of the CSL Λ^{CSL}. In fact, given a set of lattices $\Lambda^1, \Lambda^2, \ldots, \Lambda^r$, we can always easily enumerate the positions of the vertices of each of them inside C_o^{CSL} in terms of the corresponding generator matrices and check computationally whether consistency is satisfied or not.

We show in Fig. 9 examples of linear consistency in $\mathbb{R}^2$ for redundancies $r = 3, 4$, where the reconstruction vectors have been represented by "$\circ$".

B. Consistent Reconstruction Algorithms With Improved Performance

Given a regular EVQ, it is desirable for a good rate-distortion performance that the reconstructions be located near the centroids of the EVQ cells. It can be seen in Fig. 9 how the consistent linear reconstructions given by the minimal dual frames for $r = 3, 4$ are not located near the centroids corresponding to a uniform distribution. In order to achieve a better performance, it is necessary to use more intelligent (although simple and low-complexity) reconstruction algorithms which make explicit use of the periodicity property.

1) Reconstruction With a Small Lookup Table in Periodic EVQs: Given a periodic EVQ, it is possible to perform reconstruction efficiently and accurately by using a small-size lookup table scheme, which also ensures consistency. This can be done for any periodic EVQ. Let us first consider the case of tight frames composed by a set of orthogonal bases. Assume, for simplicity and without loss of generality, that $N = 2$ and let $\mathcal{P}_o$ be the smallest rectangular polytope which is a basic unit polytope for the partition defined by the EVQ. Notice that although the minimal unit cell C_o^{CSL} may not be rectangular, from Lemma 1, since Λ^1 is rectangular, it is always possible to find a rectangular polytope $\mathcal{P}_o$ (with volume larger than the volume of C_o^{CSL}) which is also a (nonminimal) basic unit polytope. The reason for choosing this basic rectangular polytope is that the reconstruction algorithm becomes even simpler in this case. Since the periodicity of the EVQ is determined by Λ^{CSL}, the smallest rectangular polytope $\mathcal{P}^{\text{CSL}}$ covering C_o^{CSL} is a valid candidate for $\mathcal{P}_o$. It is clear that, due to the periodicity determined by $\mathcal{P}^{\text{CSL}}$, any vertical or horizontal shift of $\mathcal{P}^{\text{CSL}}$ by an integer number of step sizes (Δ_1^1 is the horizontal step size and Δ_2^1 is

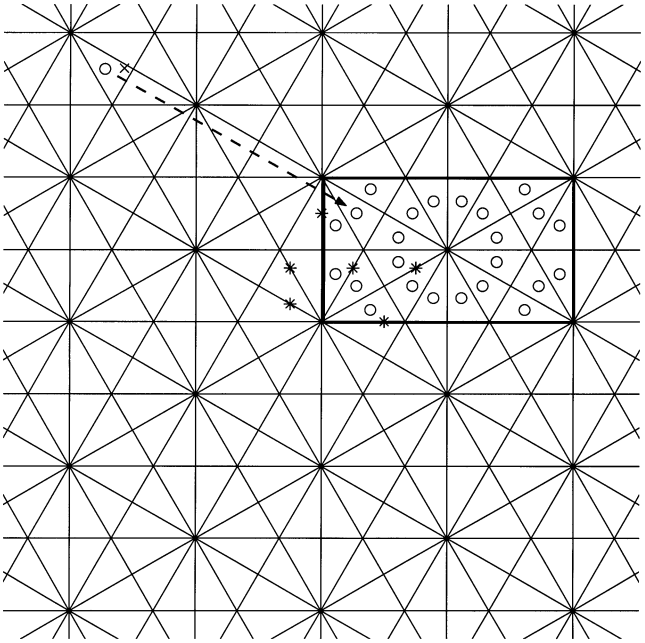

Fig. 10. Reconstruction algorithm based on lookup table: "$\circ$" represents reconstruction vectors, "$*$" the values of the quantized coefficients which define the equivalent cell in the unit cell $\mathcal{P}_o$, "$\times$" represents the input vector. All the information is first translated to the unit cell $\mathcal{P}_o$, then the reconstruction vector of the equivalent cell is read, and finally it is translated back to the proper cell. Notice that in this example, with this lookup table scheme, the EVQ cells are actually (minimum-distance) Voronoi cells.

the vertical step size) gives rise to another polytope which also keeps periodicity.

In Fig. 10, the polytope that has been chosen is indicated using bold line. Consider the polytope $\mathcal{P}_o$ and let N_1^1 and N_2^1 be the number of step sizes that determine the length of the sides (vertical and horizontal) of $\mathcal{P}_o$. For the example in Fig. 10, $N_1^1 = 2$ and $N_2^1 = 2$. Let $\boldsymbol{v}_o$ be the center of $\mathcal{P}_o$. Given any input signal $\boldsymbol{x}$, it is straightforward to find the equivalent polytope $\mathcal{P}_k$, which is a translation of $\mathcal{P}_o$ given by

$$\mathcal{P}_k = \mathcal{P}_o + n_1^1 N_1^1 \Delta_1^1 + n_2^1 N_2^1 \Delta_2^1, \quad \text{for some integers } n_1^1,\, n_2^1 \in \mathbb{Z}. \quad (43)$$

The basic idea is that given any EVQ cell C_i^{EVQ} it is possible to find very easily and quickly the equivalent cell (by equivalent cell we mean a congruent cell that is exactly equal in shape and size) which is inside $\mathcal{P}_o$. Given an input signal $\boldsymbol{x}$ whose quantized coefficients are $\boldsymbol{y}_q = \mathrm{PSQ}(\boldsymbol{y})$, where $\boldsymbol{y} = \boldsymbol{F}\boldsymbol{x}$, it is possible to translate the values of the quantized coefficients to other values $\boldsymbol{y}_q^{\mathcal{P}_o}$ which define the equivalent cell $V_{i_o}^{\mathrm{EVQ}}$ that is inside $\mathcal{P}_o$. This translation is illustrated in Fig. 10. Let $\boldsymbol{v}_k$ be the center of the polytope $\mathcal{P}_k$. In this particular case, since $\mathcal{P}_o$ is rectangular (cubic in higher dimensions), it is clear that $\boldsymbol{v}_k$ can be calculated by a simple floor operation because $\mathcal{P}_o$ is rectangular. If we let $\boldsymbol{d} = \boldsymbol{v}_o - \boldsymbol{v}_k$, then if $\hat{\boldsymbol{x}}_o$ is the reconstruction vector corresponding to $V_{i_o}^{\mathrm{EVQ}}$, the reconstruction corresponding to C_i^{EVQ} is just $\hat{\boldsymbol{x}} = \hat{\boldsymbol{x}}_{\boldsymbol{o}} - d$. The reconstruction $\hat{\boldsymbol{x}}_{\boldsymbol{o}}$ is obtained by just looking up the corresponding reconstruction vector stored in a lookup table. Notice that we can perform optimal reconstruction for the case of a uniform input distribution, because, for each EVQ cell inside $\mathcal{P}_o$, we can store a vector obtained by averaging over all the vertices (extreme points) of the cell (barycenter of the cell), which can be shown to be exactly equal to the centroid of the corresponding (convex) cell assuming a uniform distribution [25]. In the example shown in Fig. 10, the needed lookup table consists of only 24 reconstruction vectors. The fundamental advantage provided by the periodicity is that if the periodic EVQ is well designed, the size of the lookup table can be made small, and does not increase with the rate of the EVQ. Notice also that for this example, with the reconstructions given by the lookup table, the EVQ cells are actually (minimum-distance) Voronoi cells. For the case of arbitrary EVQs, a valid polytope $\mathcal{P}_o$ is always given by C_o^{CSL} and a similar reconstruction procedure can be followed. Now, $\boldsymbol{v}_k$ will be calculated by quantizing with respect to Λ^{CSL} which will not be, in general, a rectangular lattice. For instance, for those periodic EVQs based on hexagonal lattices in $\mathbb{R}^2$, a valid polytope $\mathcal{P}_o$ will be an hexagonal cell. For instance, in Fig. 8, a valid $\mathcal{P}_o$ is illustrated.

Because of the periodicity in the structure of any periodic EVQ, the information can be easily encoded in an embedded (successive) manner by dividing it into two parts, the entropy associated with the cells $\{\mathcal{P}_k\}$, and the conditional entropy associated with the structure of cells that is inside each $\mathcal{P}_k$, which is the same structure as in $\mathcal{P}_o$. In Fig. 10, for instance, given a certain polytope $\mathcal{P}_k$, which can be found by quantizing the coefficients $\{y_1^1, y_2^1\}$, respectively, with step sizes $2\Delta_1^1$ and $2\Delta_2^1$ (this can be viewed as a coarse prequantization), the only additional information that has to be stored to encode a vector is an index between 1 and 24.

The vectors of the lookup table can be easily calculated in any dimension N by using LP. In order to do so, for each EVQ cell in the polytope $\mathcal{P}_o$, we run a large enough number of linear programs with different cost vectors pointing in different directions in $\mathbb{R}^N$ and where the constraints are such that they define the specific EVQ cell in terms of inequality constraints. This allows us to calculate all the vertices of the corresponding EVQ cell and by taking the average we obtain a good approximation of its centroid. Moreover, it is not necessary to calculate the vectors of the lookup table for each rate of the EVQ because, by linearity, all the vertices scale their coordinates linearly and simultaneously with Δ_1^1. Therefore, we only need to calculate these vectors *once* for the rate corresponding to $\Delta_1^1 = 1$. This procedure is explained in greater detail in [22].

2) Improved Linear Reconstruction in Periodic EVQs With Spherical Symmetry: It is also possible to design periodic EVQs with additional symmetry properties so that a very simple improved linear reconstruction algorithm can be used to obtain reconstructions that are located near the centroids of the EVQ cells (assuming a uniform distribution). Let us consider a periodic EVQ that satisfies the following two properties.

1) It is consistent under the usual linear reconstruction using the minimal dual frame.
2) These linear reconstruction vectors are located with circular symmetry (spherical symmetry for $N > 2$) with respect to the lattice points of either the CSL Λ^{CSL} or a coset (translation) of it.

Several examples have been found where this circular symmetry is satisfied, as for instance, the two examples shown in

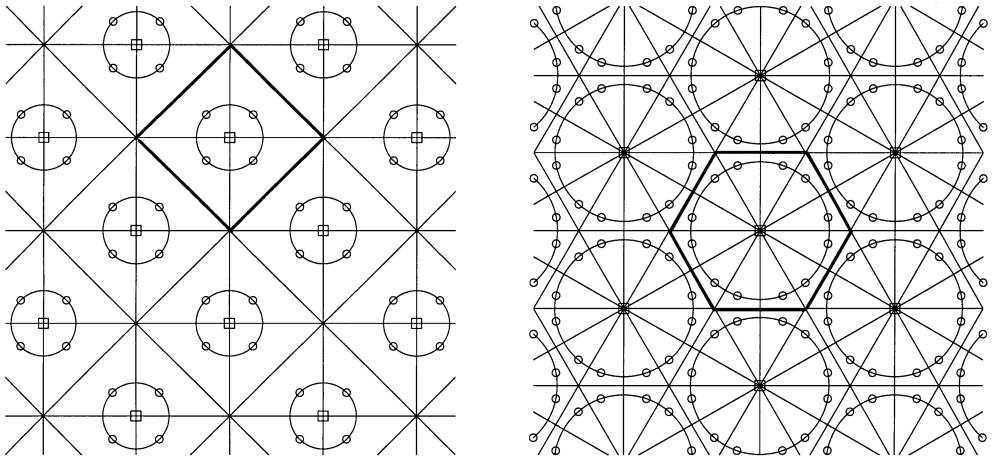

(a) (b)

Fig. 11. Examples of circular symmetry in $\mathbb{R}^2$: (a) $r = 2$. Squares represent the lattice points of a coset of Λ^{CSL}. (b) $r = 3$. Squares represent the lattice points of Λ^{CSL}.

Fig. 11 for redundancies $r = 2$ and $r = 3$, and the example 4 for dimension $N = 4$ and $r = 3$. The circular symmetry makes it simple to design a perturbation so that the reconstruction vectors that are obtained are close to the centroids with respect to a uniform distribution.

Let $\hat{\boldsymbol{x}}_{\mathrm{LQ}}$ be the reconstruction given by a usual lattice quantizer with reproduction vectors given by the points of the CSL or a translation of it. For the examples shown in Fig. 11, the points of these lattices are represented by squares and one of the Voronoi cells is also highlighted with bold lines. It is very simple to improve the linear reconstruction given by the minimal dual frame by performing a perturbation

$$\hat{\boldsymbol{x}} = \hat{\boldsymbol{x}}_{\mathrm{MD}} + \delta\Delta_1^1(\hat{\boldsymbol{x}}_{\mathrm{MD}} - \hat{\boldsymbol{x}}_{\mathrm{LQ}}) \tag{44}$$

where $\hat{\boldsymbol{x}}_{\mathrm{MD}}$ is the reconstruction given by the minimal dual frame and the direction of the perturbation is determined by the difference vector $\boldsymbol{d} = \hat{\boldsymbol{x}}_{\mathrm{MD}} - \hat{\boldsymbol{x}}_{\mathrm{LQ}}$. Thus, the magnitude of the perturbation is $\|\boldsymbol{d}\|\delta\Delta_1^1$ and the value of δ has to be chosen appropriately so that the final reconstruction $\hat{\boldsymbol{x}}$ is as close as possible to the centroid of the cell. Note that once the best value for δ has been chosen, this is fixed and independent of the input vector $\boldsymbol{x}$ and the scaling of the lattices changes only Δ_1^1. The main advantage of this method with respect to the lookup table scheme is that we do not need a lookup table to store the reproduction vectors of the cells contained inside the minimal periodic unit of the tesselation. However, further research is necessary in order to understand what are the necessary and sufficient conditions which ensure that the property of circular symmetry is satisfied.

V. Numerical Results for Some Periodic EVQ Designs and Applications

Our designs are more suitable to be used for small redundancies and low to moderate dimensions, and have a complexity similar to the usual linear reconstruction. At high redundancies, it is always possible to find designs but they may not be very efficient in terms of coding due to the number of constraints in the quantization step sizes that have to be met and also the number of reproductions which have to be stored in the lookup table may be large. However, note that for some important applications, such as those involving very high-frequency analog signals (e.g., optical signals), it is usually not feasible to use redundancies higher than $r = 3$ or $r = 4$. Moreover, there exist also other systems called Polyphase A/D converters [38], [39] that divide the bandwidth of the input signal into different narrow subbands (low dimension), and use a different low-rate A/D converter for each of the subband signals, that is, where each of these A/D converters works at a low oversampling ratio. Our system can also be designed theoretically for many different dimensions as shown by Sloane and Beferull-Lozano in [22] but the generated tesselations can become very complicated for dimensions $N > 8$ and the number of elements in the lookup table is also large. For $N \leq 8$, it is possible to find constructions such that the number of different cells (number of elements in the lookup table) is sufficiently small.

We have compared the rate-distortion performance of a) usual linear reconstruction (minimal dual frame) with a nonperiodic EVQ with equal quantization step sizes, that is, the quantization system used in all the previous work; b) reconstruction based on a periodic EVQ with different quantization step sizes using either the lookup table scheme or the improved linear reconstruction (their difference in performance is negligible in these examples); and c) usual linear reconstruction (minimal dual frame) used with a periodic EVQ with different quantization step sizes. The bit rate associated with the quantized tight frame coefficients is obtained by measuring the joint entropy of all these quantized coefficients, and the distortion is measured in terms of the MSE. The input source that has been used is a 2-D Gaussian distribution $\mathcal{N}(\boldsymbol{0}, \sigma^2\boldsymbol{I})$ with $\sigma = 0.3$. The periodic EVQs that have been used are the ones shown in Figs. 11(a) and 6(a), respectively, for $r = 2$ and $r = 3$. For these two examples, the rate-distortion performances of the lookup table scheme and the improved linear reconstruction using a periodic EVQ are approximately the same because the reconstructions can be taken to be practically the same and obviously, the associated rate is also the same.

It can be seen in Fig. 12 that the best performance is clearly achieved by the lookup table and the improved linear recon-

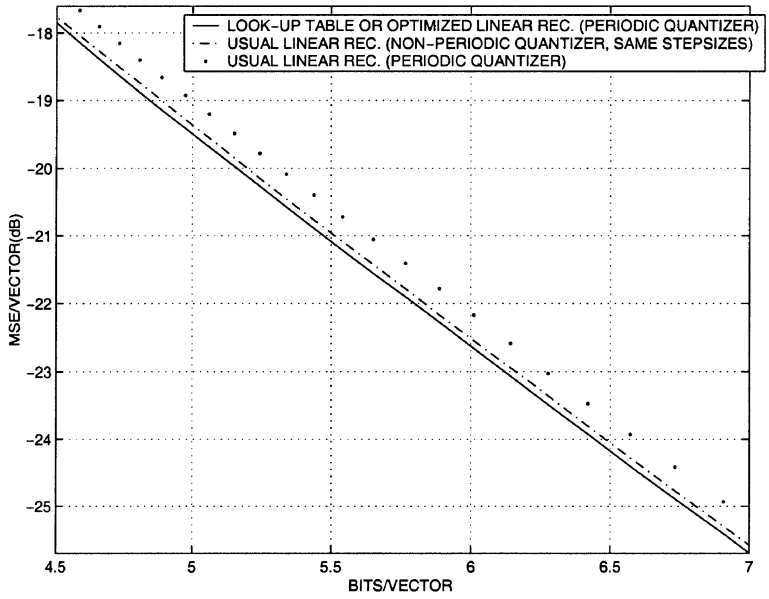

(a)

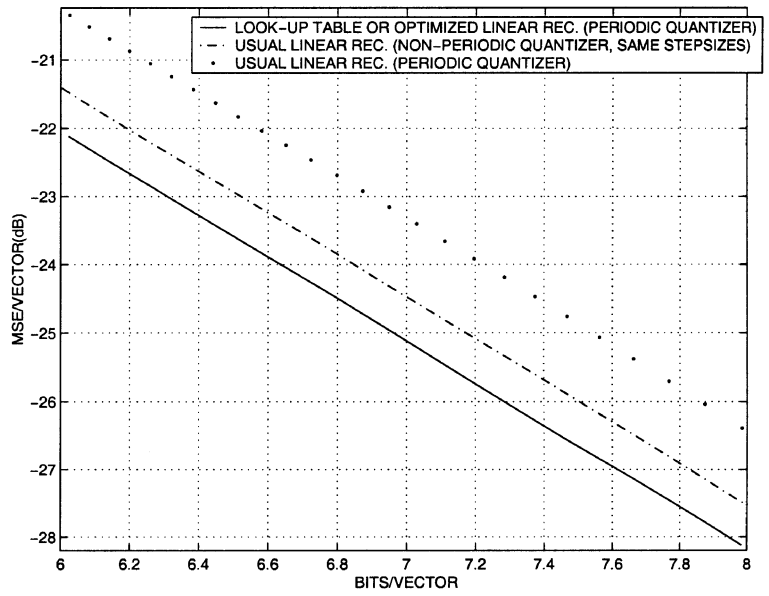

(b)

Fig. 12. Comparison, for a 2-D uncorrelated Gaussian source, of 1) usual linear reconstruction with a nonperiodic quantizer with equal quantization step sizes (classic system); 2) reconstruction in a periodic EVQ with different quantization step sizes using either the lookup table scheme or the improved linear reconstruction (the difference in performance for these two systems is negligible for these examples); 3) usual linear reconstruction in a periodic quantizer with different quantization step sizes. The values of MSE are given per vector in decibels and the bit rate is given in bits per vector. Part (a) corresponds to the example shown in Fig. 11(a) with $r = 2$ and part (b) corresponds to the example shown in Fig. 6(a) with $r = 3$

struction systems, with a gain of around 0.2 dB for $r = 2$ and a gain of around 0.7 dB for $r = 3$ over the classic system that uses linear reconstruction and the same quantization step sizes.

At the same time, Fig. 12 also shows clearly the fact that, a linearly consistent EVQ does not necessarily yield a better rate-distortion performance than a *different* linearly nonconsistent EVQ$'$ at the same rate, that is, by enforcing a periodic structure we may get a quantizer with worse performance than another quantizer whose structure results in linear inconsistency; however, when we use a periodic EVQ and enforce the consistent reconstructions to be sufficiently close to the real centroids by using our reconstruction methods, the periodic EVQ achieves, in all cases, a superior performance over the nonperiodic EVQ.

A. Implications for Oversampled A/D Conversion

It can be shown that the oversampling of a periodic band-limited signal can be expressed as a frame operator in $\mathbb{R}^N$ whose input are the Fourier coefficients (finite discrete Fourier expansion) of the signal that is sampled [4]. As a particular illustrative case, if we consider the space of sinusoids of period T spanned by $\{\cos(2\pi t/T), \sin(2\pi t/T)\}$, the sampling and uniform scalar quantization in amplitude of these signals is equivalent to the quantization of an overcomplete expansion (frame) in

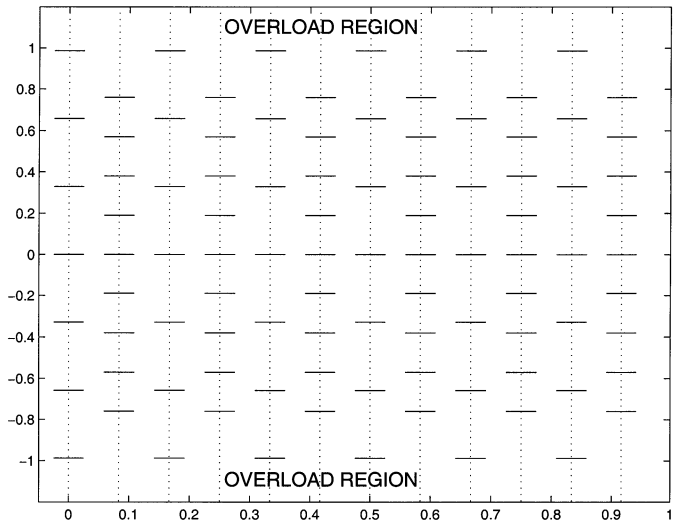

Fig. 13. Scalar quantizers (time domain) corresponding to the EVQ in Fig. 6(a).

$\mathbb{R}^2$. Each sampling time t_i is directly associated with the vector $\boldsymbol{\varphi_i} = [\cos(2\pi t_i/T), \sin(2\pi t_i/T)]$ and all these vectors define the equivalent frame in $\mathbb{R}^2$. Moreover, by Parseval's theorem, we have that

$$\text{MSE} = ||\hat{y}(t) - y(t)||_T^2 = ||\hat{\boldsymbol{x}} - \boldsymbol{x}||^2$$

where $\hat{y}(t)$ is the reconstructed sinusoid, that is, the MSE of the reconstructed sinusoidal signal in the converter is the same as the MSE that occurs on the frame domain. Thus, given a tight frame in $\mathbb{R}^2$ together with a set of different step sizes such that a periodic EVQ is obtained, if we translate the values of angles to sampling times, we can obtain the scalar quantizers that are applied at the corresponding sampling times. For instance, the quantizer in Fig. 6(a) gives rise to a converter with uniform sampling in time and with two different scalar quantizers, one with a step size larger than the other one (see Fig. 13).

VI. Conclusion

The basic results presented in this paper are as follows. We study the problem of achieving consistency in quantized overcomplete expansions with low-complexity algorithms. Consistency leads to EVQs which are regular. In order to achieve this goal, we allow the use of different step sizes in the scalar quantization of the expansion coefficients and construct EVQs having cells with a periodic structure. Periodic quantizers are defined in terms of lattices and sublattices with certain properties and we give various design examples based on different tight frames. On the one hand, we show that periodicity is a necessary condition to have consistency under simple linear reconstruction. On the other hand, a periodic structure makes it possible to reconstruct efficiently and accurately using either a small lookup table whose size does not increase with the rate of the quantizer or using a simple improved linear reconstruction for periodic EVQs with certain convenient structural properties. Regarding future work, it should be noticed that further research is needed in order to make it possible to apply our approach to A/D conversion of arbitrary band-limited signals.

Appendix I
Proof of Fact 1

Since $S\Lambda$ is a sublattice of Λ^1, $S\Lambda$ is a subgroup of the additive group Λ^1, and the result follows directly by group theory. The periodicity is determined by the subgroup and, therefore, the minimal periodic unit is given by the tiling contained in $C_o^{S\Lambda}$, the fundamental polytope associated with the sublattice $S\Lambda$. Since the subgroup structure is true for any dimension N, the periodicity property is also true for any dimension N. □

Appendix II
Proof of Lemma 1

Let $\boldsymbol{M}_{\Lambda^j} = \boldsymbol{A}_{\Lambda^j}\boldsymbol{M}_{\Lambda^1}$ and consider the matrix $\boldsymbol{A}_{\Lambda^j}$ given by

$$\boldsymbol{A}_{\Lambda^j} = \begin{pmatrix} \frac{1}{d_1^j} & 0 \\ 0 & \frac{1}{d_2^j} \end{pmatrix} \begin{pmatrix} k_{11}^j & k_{12}^j \\ -k_{21}^j & k_{22}^j \end{pmatrix} \tag{45}$$

whose inverse is equal to

$$\begin{aligned}(\boldsymbol{A}_{\Lambda^j})^{-1} &= \frac{1}{k_{11}^j k_{22}^j + k_{12}^j k_{21}^j} \begin{pmatrix} k_{22}^j d_1^j & k_{12}^j d_2^j \\ -k_{21}^j d_1^j & k_{11}^j d_2^j \end{pmatrix} \\ &= \frac{1}{D^j} \begin{pmatrix} t_{11}^j & t_{12}^j \\ t_{21}^j & t_{22}^j \end{pmatrix}\end{aligned} \tag{46}$$

where $t_{lm}^j \in \mathbb{Z}$ and $D^j \in \mathbb{Z}_+$ is the denominator that is left after all the common factors have been canceled out. For each j, we define the lattice $\Lambda^{j'}$ with generator matrix given by

$$\boldsymbol{M}_{\Lambda^{j'}} = D^j(\boldsymbol{A}_{\Lambda^j})^{-1}\boldsymbol{M}_{\Lambda^j} = D^j(\boldsymbol{A}_{\Lambda^j})^{-1}\boldsymbol{A}_{\Lambda^j}\boldsymbol{M}_{\Lambda^1} = D^j\boldsymbol{M}_{\Lambda^1}. \tag{47}$$

Notice that $\Lambda^{j'} \subset \Lambda^j$ is a sublattice of Λ^j because the matrix $D^j(\boldsymbol{A}_{\Lambda^j})^{-1}$ has integer entries. Let $\text{l.c.m.}\,(a_1, a_2, \ldots, a_r)$ be the *least common multiple* of $a_1, a_2, \ldots, a_r$, that is, the smallest positive integer that all $a_1, a_2, \ldots, a_r$ divide. After calculating $\boldsymbol{M}_{\Lambda^{j'}}\ \forall j = 1, \ldots, r$, we define D as

$$D = \text{l.c.m}\,(D^1, D^2, \ldots, D^r)$$

and the lattice Λ^o with generator matrix $\boldsymbol{M}_{\Lambda^o} = D\boldsymbol{M}_{\Lambda^1}$, which means that Λ^o is an integer scaling of Λ^1. Thus, we have that $\Lambda^o \subset \Lambda^{j'} \subset \Lambda^j \subset \Lambda^1, \forall j = 1, \ldots, r$. This implies clearly that $\Lambda^o \subset (\Lambda^1 \cap \Lambda^2 \cap \cdots \cap \Lambda^r)$ and, therefore, Λ^o is a sublattice of the CSL Λ^{CSL}. □

Appendix III
Proof of Lemma 2

Since Λ^{CSL} is the finest sublattice of all the lattices Λ^j, $j = 1, \ldots, r$, if we consider any cell C_i^{CSL}, the relative positions of the lattice points $\{\boldsymbol{v}_i^j\}$ (vertices of the cells associated with Λ^j) for each lattice Λ^j, which are inside the cell C_i^{CSL}, these positions are always the same independently of which cell C_i^{CSL} is chosen. This immediately implies that the structure of the resulting EVQ is a periodic repetition of the structure of cells that is inside the fundamental polytope C_o^{CSL} of the CSL. □

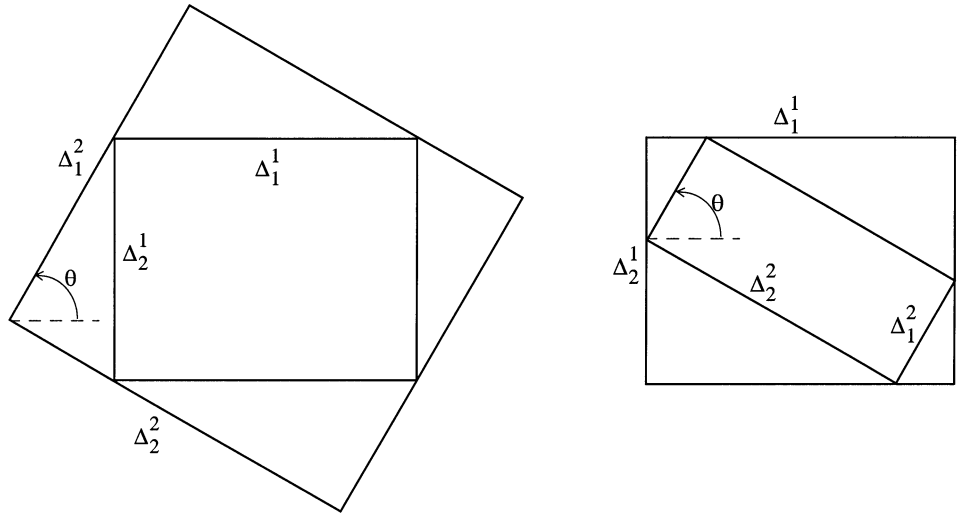

Fig. 14. Two limiting cases for the step sizes Δ_1^2 and Δ_2^2 of the quantizer Q^2.

Appendix IV
Proof of Fact 2

The proof follows in a straightforward manner by direct calculation from the definition of sublattice, which implies that

$$\begin{pmatrix} c_1\Delta_1^1 & 0 \\ 0 & c_2\Delta_2^1 \end{pmatrix}\begin{pmatrix} \cos(\theta) & \sin(\theta) \\ -\sin(\theta) & \cos(\theta) \end{pmatrix} = \begin{pmatrix} k_{11}\Delta_1^1 & k_{12}\Delta_2^1 \\ -k_{21}\Delta_1^1 & k_{22}\Delta_2^1 \end{pmatrix}. \quad (48)$$

Hence, a set of sufficient conditions is given by

$$\begin{aligned} c_1\Delta_1^1[\cos(\theta), \sin(\theta)] &= [k_{11}\Delta_1^1, k_{12}\Delta_2^1] \\ c_2\Delta_2^1[-\sin(\theta), \cos(\theta)] &= [-k_{21}\Delta_1^1, k_{22}\Delta_2^1], \\ & k_{11}, k_{12}, k_{21}, k_{22} \in \mathbb{Z}. \end{aligned} \quad (49)$$

If we use the variable $\beta = \frac{\Delta_2^1}{\Delta_1^1}$ and simplify the previous equations, we get that

$$c_1\cos(\theta) = k_{11} \quad (50)$$
$$c_1\sin(\theta) = \beta k_{12} \quad (51)$$
$$-c_2\beta\sin(\theta) = -k_{21} \quad (52)$$
$$c_2\cos(\theta) = k_{22}. \quad (53)$$

Without loss of generality, we consider the case $0 < \theta < \frac{\pi}{2}$. This constrains the signs of all the integers k_{11}, k_{12}, k_{21}, and k_{22} to be positive. Solving the previous equations for β and θ results in

$$\beta = \sqrt{\frac{k_{11}k_{21}}{k_{12}k_{22}}}, \qquad \tan(\theta) = \sqrt{\frac{k_{12}k_{21}}{k_{11}k_{22}}}. \quad (54)$$

The values for c_1 and c_2 follow from (50) and (51).

Appendix V
Geometric Constraints on the Step Sizes

Let us consider for simplicity the case of $r = 2$. The approach we have followed is to constrain the possible step sizes Δ_1^2, Δ_2^2 to have values between the two limiting cases that happen when the Voronoi region of one quantizer is totally inside of a Voronoi cell of the other quantizer, as shown in Fig. 14. These two limiting cases establish upper and lower bounds for the pair (d_1^2, d_2^2) such that all pairs in between will satisfy the property. By using elemental trigonometry, we can calculate upper and lower bounds for the pair (d_1^2, d_2^2).

From Fig. 14(a), we get that

$$\begin{aligned} \Delta_2^1\sin(\theta) + \Delta_1^1\cos(\theta) \geq \Delta_1^2 &\Longrightarrow d_1^2 \geq \frac{k_{11}^2k_{22}^2 + k_{12}^2k_{21}^2}{k_{21}^2 + k_{22}^2} \\ \Delta_1^1\sin(\theta) + \Delta_2^1\cos(\theta) \geq \Delta_2^2 &\Longrightarrow d_2^2 \geq \frac{k_{11}^2k_{22}^2 + k_{12}^2k_{21}^2}{k_{11}^2 + k_{12}^2} \end{aligned} \quad (55)$$

which gives lower bounds for d_1^2 and d_2^2.

In the same way, from Fig. 14(b), we get that

$$\begin{aligned} \Delta_1^2\sin(\theta) + \Delta_2^2\cos(\theta) \geq \Delta_2^1 &\Longrightarrow \frac{k_{12}^2}{d_1^2} + \frac{k_{22}^2}{d_2^2} \geq 1 \\ \Delta_2^2\sin(\theta) + \Delta_1^2\cos(\theta) \geq \Delta_1^1 &\Longrightarrow \frac{k_{11}^2}{d_1^2} + \frac{k_{21}^2}{d_2^2} \geq 1 \end{aligned} \quad (56)$$

which gives upper bounds for d_1^2 and d_2^2.

For instance, in Example 1, the pairs (d_1^2, d_2^2) are constrained by

$$\begin{aligned} d_1^2 \geq \tfrac{7}{4}, \qquad & d_2^2 \geq \tfrac{7}{3} \\ 2d_2^2 + d_1^2 \geq d_1^2d_2^2, \qquad & 3d_1^2 + d_2^2 \geq d_1^2d_2^2 \end{aligned} \quad (57)$$

which limits the possible values of (d_1^2, d_2^2) to

$$\{(2,3), (2,4), (2,5), (2,6), (2,7), (3,3)\}.$$

Appendix VI
Proof of Lemma 3

By adding and subtracting (38) and (39), and doing the same for (40) and (41), we get the following equivalent set of equations:

$$\Delta_1^2\cos(\theta) = \frac{q_1 + q_2}{2}\,\Delta_1^1 = q_1'\Delta_1^1 \quad (58)$$
$$\Delta_2^2\sin(\theta) = \frac{q_2 - q_1}{2}\,\Delta_1^1 = q_2'\Delta_1^1 \quad (59)$$
$$\Delta_1^2\sin(\theta) = \frac{q_3 + q_4}{2}\,\Delta_2^1 = q_3'\Delta_2^1 \quad (60)$$

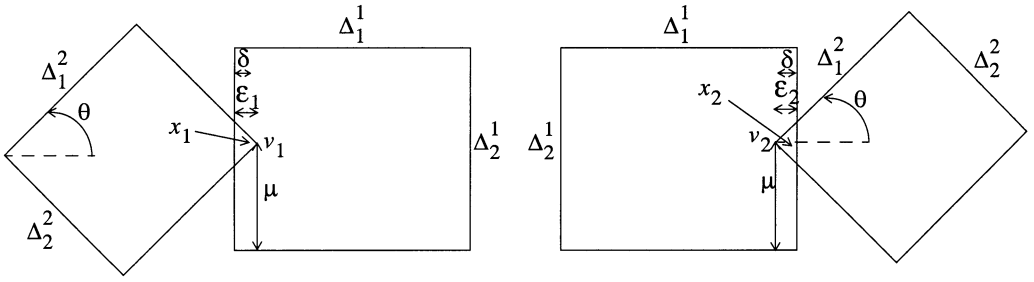

Fig. 15. Case 1 (Case 2 is Case 1 rotated 90°) in the proof of the Theorem. It is not possible (if the EVQ is not periodic) to keep linear consistency simultaneously in the two (small) EVQ cells shown.

$$\Delta_2^2 \cos(\theta) = \frac{q_3 - q_4}{2}\,\Delta_2^1 = q_4' \Delta_2^1 \quad \text{with } q_1',\, q_2',\, q_3',\, q_4' \in \mathbb{Q}. \tag{61}$$

Assume that (58)–(61) are satisfied. Manipulating these equations, we get

$$\text{Dividing (58) and (59),}\ \tan(\theta) = \frac{\Delta_1^2}{\Delta_2^2}\,\frac{q_2'}{q_1'} \tag{62}$$

$$\text{Dividing (60) and (61),}\ \tan(\theta) = \frac{\Delta_2^2}{\Delta_1^2}\,\frac{q_3'}{q_4'} \tag{63}$$

$$\text{Dividing (58) and (61),}\quad \frac{\Delta_1^2}{\Delta_2^2} = \frac{\Delta_1^1}{\Delta_2^1}\,\frac{q_1'}{q_4'} \tag{64}$$

$$\text{Dividing (59) and (60),}\quad \frac{\Delta_1^2}{\Delta_2^2} = \frac{\Delta_2^1}{\Delta_1^1}\,\frac{q_1'}{q_4'}. \tag{65}$$

Solving these equations and expressing all the step sizes in terms of Δ_1^1 we obtain

$$\tan(\theta) = \sqrt{\frac{q_2' q_3'}{q_1' q_4'}} \tag{66}$$

$$\Delta_2^1 = \beta \Delta_1^1 = \sqrt{\frac{q_1' q_2'}{q_3' q_4'}}\,\Delta_1^1 \tag{67}$$

$$\Delta_1^2 = \frac{q_1'}{\cos(\theta)}\,\Delta_1^1 \tag{68}$$

$$\Delta_2^2 = \sqrt{\frac{q_1' q_3'}{q_2' q_4'}}\,\Delta_1^2 = \frac{q_4'}{\cos(\theta)}\sqrt{\frac{q_1' q_2'}{q_3' q_4'}}\,\Delta_1^1 = \frac{q_4'}{\cos(\theta)}\,\beta \Delta_1^1. \tag{69}$$

If we compare (66)–(69) with (19) and (20), we have obtained exactly the same equations with $q_1' = \frac{k_{11}^2}{d_1^2}$, $q_2' = \frac{k_{21}^2}{d_2^2}$, $q_3' = \frac{k_{12}^2}{d_1^2}$, and $q_4' = \frac{k_{22}^2}{d_2^2}$. Since the final set of equations is equivalent to the first four equations (38)–(41), it is clear that this lemma is also true in the other direction. □

Appendix VII
Proof of Theorem 2

Without loss of generality, we can assume a quantizer Q^1 associated with a lattice Λ^1 where $\boldsymbol{F}^1 = \boldsymbol{I}_{2\times 2}$ and $\boldsymbol{M}_{\Lambda^1} = diag[\Delta_1^1, \Delta_2^1]$. A general quantizer Q^2 can be associated with a lattice Λ^2. We denote by $\boldsymbol{x}|_i$ the components of $\boldsymbol{x}$ expressed in the basis $\{\boldsymbol{\varphi}_1^i, \boldsymbol{\varphi}_2^i\}$, $i = 1, 2$, where $i = 1$ indicates, without loss of generality, the natural basis. In order to find an inconsistent cell, we consider the vertices of Λ^2. Any vertex can be written as

$$\boldsymbol{\omega} = k_1\left(\Delta_1^2 \boldsymbol{\varphi}_1^2 + \Delta_2^2 \boldsymbol{\varphi}_2^2\right) + k_2\left(\Delta_1^2 \boldsymbol{\varphi}_1^2 - \Delta_2^2 \boldsymbol{\varphi}_2^2\right), \quad k_1,\, k_2 \in \mathbb{Z}. \tag{70}$$

The components of these lattice points are

$$\boldsymbol{\omega}|_1 = \begin{pmatrix} k_1\left(\Delta_1^2\cos(\theta) - \Delta_2^2\sin(\theta)\right) + k_2\left(\Delta_1^2\cos(\theta) + \Delta_2^2\sin(\theta)\right) \\ k_1\left(\Delta_1^2\sin(\theta) + \Delta_2^2\cos(\theta)\right) + k_2\left(\Delta_1^2\sin(\theta) - \Delta_2^2\cos(\theta)\right) \end{pmatrix}, \quad k_1,\, k_2 \in \mathbb{Z}. \tag{71}$$

Notice that the two terms in the first component coincide with the left-hand-sides of (38) and (39) and the two terms in the second component coincide with the left-hand-sides of (40) and (41). Applying Lemma 3, if Q^2 is not constructed so that the EVQ is a periodic quantizer, that is, if

$$\boldsymbol{M}_{\Lambda^2} \neq \text{diag}\,[1/d_1^2,\, 1/d_2^2]\boldsymbol{M}_{S\Lambda^2}$$

with $S\Lambda^2$ being a geometrically scaled-similar sublattice of Λ^1, at least one of the following equations is **not** satisfied:

(first component in $\boldsymbol{w}$)

$$\Delta_1^2\cos(\theta) - \Delta_2^2\sin(\theta) = q_1\Delta_1^1 \tag{72}$$

(first component in $\boldsymbol{w}$)

$$\Delta_1^2\cos(\theta) + \Delta_2^2\sin(\theta) = q_2\Delta_1^1 \tag{73}$$

(second component in $\boldsymbol{w}$)

$$\Delta_1^2\sin(\theta) + \Delta_2^2\cos(\theta) = q_3\Delta_2^1 \tag{74}$$

(second component in $\boldsymbol{w}$)

$$\Delta_1^2\sin(\theta) - \Delta_2^2\cos(\theta) = q_4\Delta_2^1 \quad \text{where } q_1,\, q_2,\, q_3,\, q_4 \in \mathbb{Q} \tag{75}$$

that is, at least one $q_i \notin \mathbb{Q}$. We now recall one of the properties of the mod function, which is that if $z = \mu v$ where $\mu \notin \mathbb{Q}$ and $v \in \mathbb{R}$, then $\{kz \bmod v,\, k \in \mathbb{Z}\} =]0,\, v[$. In the case of having $z = qv$ with $q \in \mathbb{Q}$, then, the set $\{kz \bmod v,\, k \in \mathbb{Z}\}$ is composed only of a finite number of distinct values. This gives two cases. Case 1: if at least one of the equations (38), (39) is not satisfied, then the first (horizontal) component in (71) of the lattice points of Λ^2 can have an arbitrary value (modulo Δ_1^1) (see Fig. 15) and Case 2: if at least one of the equations (40), (41) is not satisfied, then the second (vertical) component in (71) can have an arbitrary value (modulo Δ_2^1). Notice that Case 1 and Case 2 are equivalent because the only difference between them is which coordinate fails to have a finite number of different values. Case 1 is the one that is actually represented graphically

in Fig. 15, and Case 2 corresponds to the Fig. 15 rotated 90 degrees. Thus, the proof of Case 1 and Case 2 is exactly the same, and we can consider only Case 1 without loss of generality.

Thus, consider that at least one of the equations (38), (39) is not satisfied and also let first both (40), (41) be satisfied, thus allowing a finite number of values (modulo Δ_2^1) in the second component.

Then, if we apply the previous property of the mod function, we can find a vertex $\boldsymbol{v}$ of Λ^2 of the form

$$\boldsymbol{v}|_1 = \begin{pmatrix} I_x\Delta_1^1 + \gamma \\ y \end{pmatrix}, \qquad \forall\, \gamma \in]0,\, \Delta_1^1[$$
$$\text{where } I_y\Delta_2^1 \le y < (I_y+1)\Delta_2^1 \text{ and } I_x,\, I_y \in \mathbb{Z}. \quad (76)$$

Consider now the following two input vectors $\boldsymbol{x}_1$ and $\boldsymbol{x}_2$ defined as follows:

$$\boldsymbol{x}_1|_1 = \boldsymbol{v}_1|_1 - \begin{pmatrix} \delta \\ 0 \end{pmatrix} = \begin{pmatrix} I_{x_1}\Delta_1^1 + \epsilon_1 - \delta \\ y_1 \end{pmatrix}$$
$$\boldsymbol{x}_2|_1 = \boldsymbol{v}_2|_1 + \begin{pmatrix} \delta \\ 0 \end{pmatrix} = \begin{pmatrix} (I_{x_2}+1)\Delta_1^1 - \epsilon_2 + \delta \\ y_2 \end{pmatrix} \quad (77)$$

where $\boldsymbol{v}_1 = \boldsymbol{v}_{\{\gamma=\epsilon_1\}}$, $\boldsymbol{v}_2 = \boldsymbol{v}_{\{\gamma=\Delta_1^1-\epsilon_2\}}$, $\Delta_1^1 \gg \epsilon_1$
$\epsilon_2 > 0$, $\Delta_1^1 \gg \delta > 0$, $\delta < \min(\epsilon_1, \epsilon_2)$
$I_{y_1}\Delta_2^1 \le y_1 < (I_{y_1}+1)\Delta_2^1$
$I_{y_2}\Delta_2^1 \le y_2 < (I_{y_2}+1)\Delta_2^1$
$I_{x_1}, I_{x_2}, I_{y_1}, I_{y_2} \in \mathbb{Z}$.

If we apply the quantizers Q^1 and Q^2 to the input vectors $\boldsymbol{x}_1$ and $\boldsymbol{x}_2$ and then take the average, the final reconstructions $\hat{\boldsymbol{x}}_1$ and $\hat{\boldsymbol{x}}_2$ given by the EVQ are

$$\hat{\boldsymbol{x}}_1|_1 = \begin{pmatrix} I_{x_1}\Delta_1^1 + \frac{\Delta_1^1}{4} - \frac{\Delta_1^2\cos(\theta)}{4} - \frac{\Delta_2^2\sin(\theta)}{4} + \frac{\epsilon_1}{2} \\ \frac{I_{y_1}\Delta_2^1}{2} + \frac{\Delta_2^1}{4} - \frac{\Delta_1^2\sin(\theta)}{4} + \frac{\Delta_2^2\cos(\theta)}{4} + \frac{y_1}{2} \end{pmatrix} \quad (78)$$

$$\hat{\boldsymbol{x}}_2|_1 = \begin{pmatrix} I_{x_2}\Delta_1^1 + \frac{3\Delta_1^1}{4} + \frac{\Delta_1^2\cos(\theta)}{4} + \frac{\Delta_2^2\sin(\theta)}{4} - \frac{\epsilon_2}{2} \\ \frac{I_{y_2}\Delta_2^1}{2} + \frac{\Delta_2^1}{4} + \frac{\Delta_1^2\sin(\theta)}{4} - \frac{\Delta_2^2\cos(\theta)}{4} + \frac{y_2}{2} \end{pmatrix}. \quad (79)$$

In order to be able to express the constraints to satisfy consistency along the two directions determined by the second basis $\{\boldsymbol{\varphi}_1^2, \boldsymbol{\varphi}_2^2\}$, we also express $\hat{\boldsymbol{x}}_1$ and $\hat{\boldsymbol{x}}_2$ with their components given with respect to this second basis (this is actually equivalent to a clockwise rotation of the plane by an angle of θ) as shown in (80) and (81) at the bottom of the page. For notational convenience, assume that the symbols $\le, <$ are component-wise relation symbols. Then, all the constraints that have to be satisfied to achieve consistency are given by the following component-wise inequalities:

$$\begin{pmatrix} I_{x_1}\Delta_1^1 \\ I_{y_1}\Delta_2^1 \end{pmatrix} \le \hat{\boldsymbol{x}}_1|_1 < \begin{pmatrix} I_{x_1}\Delta_1^1 + \Delta_1^1 \\ I_{y_1}\Delta_2^1 + \Delta_2^1 \end{pmatrix} \quad (82)$$

$$\begin{pmatrix} I_{x_2}\Delta_1^1 \\ I_{y_2}\Delta_2^1 \end{pmatrix} \le \hat{\boldsymbol{x}}_2|_1 < \begin{pmatrix} I_{x_2}\Delta_1^1 + \Delta_1^1 \\ I_{y_2}\Delta_2^1 + \Delta_2^1 \end{pmatrix} \quad (83)$$

$$\boldsymbol{v}_1|_2 - \begin{pmatrix} \Delta_1^2 \\ 0 \end{pmatrix} \le \hat{\boldsymbol{x}}_1|_2 < \boldsymbol{v}_1|_2 + \begin{pmatrix} 0 \\ \Delta_2^2 \end{pmatrix} \quad (84)$$

$$\boldsymbol{v}_2|_2 - \begin{pmatrix} 0 \\ \Delta_2^2 \end{pmatrix} \le \hat{\boldsymbol{x}}_2|_2 < \boldsymbol{v}_2|_2 + \begin{pmatrix} \Delta_1^2 \\ 0 \end{pmatrix} \quad (85)$$

where

$$\boldsymbol{v}_1|_2 = \begin{pmatrix} \cos(\theta)I_{x_1}\Delta_1^1 + \sin(\theta)y_1 + \cos(\theta)\epsilon_1 \\ -\sin(\theta)I_{x_1}\Delta_1^1 + \cos(\theta)y_1 - \sin(\theta)\epsilon_1 \end{pmatrix}$$
$$\boldsymbol{v}_2|_2 = \begin{pmatrix} \cos(\theta)(I_{x_2}+1)\Delta_1^1 + \sin(\theta)y_2 - \cos(\theta)\epsilon_2 \\ -\sin(\theta)(I_{x_2}+1)\Delta_1^1 + \cos(\theta)y_2 + \sin(\theta)\epsilon_2 \end{pmatrix}.$$

From the first component inequality in either (82) or (83), and using the fact that $\epsilon_1 > 0$ and $\epsilon_2 > 0$ can be taken as small as we want, we get the following lower bound for Δ_1^1:

$$\Delta_1^1 \ge \Delta_1^2\cos(\theta) + \Delta_2^2\sin(\theta). \quad (86)$$

Similarly, from (84) and (85), we can obtain, after operating, lower bounds for Δ_1^2 and Δ_2^2. Let $\mu_i = y_i \bmod \Delta_2^1$, $i = 1, 2$, that is, $\mu_1 = y_1 - I_{y_1}\Delta_2^1$ and $\mu_2 = y_2 - I_{y_2}\Delta_2^1$. The actual lower bounds for Δ_1^2 and Δ_2^2 depend on the parameters μ_1 and μ_2

$$\Delta_1^2 \ge \Delta_1^1\cos(\theta) + \Delta_2^1\sin(\theta) - 2\sin(\theta)\mu_1 \quad \left(\text{tightest if } \mu_1 \le \frac{\Delta_2^1}{2}\right) \quad (87)$$

$$\Delta_2^2 \ge \Delta_1^1\sin(\theta) + \Delta_2^1\cos(\theta) - 2\cos(\theta)\mu_2 \quad \left(\text{tightest if } \mu_2 \le \frac{\Delta_2^1}{2}\right) \quad (88)$$

$$\Delta_1^2 \ge \Delta_1^1\cos(\theta) - \Delta_2^1\sin(\theta) + 2\sin(\theta)\mu_2 \quad \left(\text{tightest if } \mu_2 \ge \frac{\Delta_2^1}{2}\right) \quad (89)$$

$$\Delta_2^2 \ge \Delta_1^1\sin(\theta) - \Delta_2^1\cos(\theta) + 2\cos(\theta)\mu_1 \quad \left(\text{tightest if } \mu_1 \ge \frac{\Delta_2^1}{2}\right). \quad (90)$$

We show next that it is always possible to find points $\boldsymbol{x}_1$ and $\boldsymbol{x}_2$ such that $\mu_1 = \mu_2$. Since (74) and (75) are satisfied, let $q_3 = \frac{n_1}{m_1}$ and $q_4 = \frac{n_2}{m_2}$, such that $\gcd(n_1, m_1) = 1$ and $\gcd(n_2, m_2) = 1$. Then, we have that

$$\begin{aligned} &\{k_1(\Delta_1^2\sin(\theta) + \Delta_2^2\cos(\theta)) \\ &\quad + k_2(\Delta_1^2\sin(\theta) - \Delta_2^2\cos(\theta)) \bmod \Delta_2^1,\, k_1,\, k_2 \in \mathbb{Z}\} \\ &\quad = \left\{0,\, \frac{\Delta_2^1}{m_1m_2},\, \frac{2\Delta_2^1}{m_1m_2},\, \ldots,\, \frac{(m_1m_2-1)\Delta_2^1}{m_1m_2}\right\}. \end{aligned} \quad (91)$$

$$\hat{\boldsymbol{x}}_1|_2 = \begin{pmatrix} I_{x_1}\Delta_1^1\cos(\theta) + \frac{I_{y_1}\Delta_2^1\sin(\theta)}{2} + \frac{\Delta_1^1\cos(\theta)}{4} + \frac{\Delta_2^1\sin(\theta)}{4} - \frac{\Delta_1^2}{4} + \frac{\sin(\theta)y_1}{2} + \frac{\cos(\theta)\epsilon_1}{2} \\ -I_{x_1}\Delta_1^1\sin(\theta) + \frac{I_{y_1}\Delta_2^1\cos(\theta)}{2} - \frac{\Delta_1^1\sin(\theta)}{4} + \frac{\Delta_2^1\cos(\theta)}{4} + \frac{\Delta_2^2}{4} + \frac{\cos(\theta)y_1}{2} - \frac{\sin(\theta)\epsilon_1}{2} \end{pmatrix} \quad (80)$$

$$\hat{\boldsymbol{x}}_2|_2 = \begin{pmatrix} I_{x_2}\Delta_1^1\cos(\theta) + \frac{I_{y_2}\Delta_2^1\sin(\theta)}{2} + \frac{3\Delta_1^1\cos(\theta)}{4} + \frac{\Delta_2^1\sin(\theta)}{4} + \frac{\Delta_1^2}{4} + \frac{\sin(\theta)y_2}{2} - \frac{\cos(\theta)\epsilon_2}{2} \\ -I_{x_2}\Delta_1^1\sin(\theta) + \frac{I_{y_2}\Delta_2^1\cos(\theta)}{2} - \frac{3\Delta_1^1\sin(\theta)}{4} + \frac{\Delta_2^1\cos(\theta)}{4} - \frac{\Delta_2^2}{4} + \frac{\cos(\theta)y_2}{2} + \frac{\sin(\theta)\epsilon_2}{2} \end{pmatrix}. \quad (81)$$

This directly implies that we can always (by varying k_1 and k_2 in (91)) find two vertices $\boldsymbol{v}_1$ and $\boldsymbol{v}_2$ (satisfying that $\mu_1 = \mu_2 = \mu$) of the following form:

$$\boldsymbol{v}_1|_1 = \begin{pmatrix} I_{x_1}\Delta_1^1 + \epsilon_1 \\ I_{y_1}\Delta_2^1 + \mu \end{pmatrix} \qquad \boldsymbol{v}_2|_1 = \begin{pmatrix} (I_{x_2}+1)\Delta_1^1 - \epsilon_2 \\ I_{y_2}\Delta_2^1 + \mu \end{pmatrix}. \tag{92}$$

Consider now the case that at least one of the equations (74), (75) were not satisfied. Then, it is also clear that we could find cells with values of μ_1 and μ_2 as close to each other as wanted because we have a continuum of values (modulo Δ_2^1) in this component, and the same conclusions in the proof would follow.

Consider first the case of $\mu_1 = \mu_2 = \mu \leq \frac{\Delta_2^1}{2}$. In this case, if we multiply (87) and (88) by $\cos(\theta)$ and $\sin(\theta)$, respectively, and then we sum them, making use of the equality $\cos^2(\theta) + \sin^2(\theta) = 1$, we obtain an upper bound for Δ_1^1 given by

$$\Delta_1^1 \leq \Delta_1^2 \cos(\theta) + \Delta_2^2 \cos(\theta) + \sin(2\theta)(2\mu - \Delta_2^1). \tag{93}$$

In order for the upper (93) and lower (86) bounds of Δ_1^1 to be consistent,[5] it is necessary to have $\mu \geq \frac{\Delta_2^1}{2}$, which implies that the only valid value for μ is $\mu = \frac{\Delta_2^1}{2}$. Consider now the case of $\mu_1 = \mu_2 = \mu \geq \frac{\Delta_2^1}{2}$. In the same way, if we multiply (89) and (90) by $\cos(\theta)$ and $\sin(\theta)$, respectively, and we sum them, we obtain an upper bound for Δ_1^1 given by

$$\Delta_1^1 \leq \Delta_1^2 \cos(\theta) + \Delta_2^2 \sin(\theta) + \sin(2\theta)(\Delta_2^1 - 2\mu). \tag{94}$$

As before, for the upper (94) and lower (87) bounds to be consistent, we need $\mu \leq \frac{\Delta_2^1}{2}$, which implies again that $\mu = \frac{\Delta_2^1}{2}$. Thus, in order to achieve consistency simultaneously for the input vectors $\boldsymbol{x}_1$ and $\boldsymbol{x}_2$, as defined in (92), it is necessary to have always $\mu = \frac{\Delta_2^1}{2}$. But this is clearly impossible because, for instance, by taking vertices with k_1, k_2 given by $k_1 = l_1 m_1$ and $k_2 = l_2 m_2$, $l_1, l_2 \in \mathbb{Z}$ in (91), we have always $\mu = 0$. Therefore, we conclude that it is impossible to achieve consistency for the two input vectors $\boldsymbol{x}_1$ and $\boldsymbol{x}_2$ simultaneously. □

ACKNOWLEDGMENT

The authors wish to thank Dr. Z. Cvetković for several helpful comments that improved substantially the clarity of the paper, and to Dr. N. J. A. Sloane, Dr. S. Diggavi, Prof. R. Guralnick, and Prof. V. Kumar for fruitful discussions about lattices. Finally, we would like to thank the anonymous reviewers for their very valuable comments.

REFERENCES

[1] Z. Cvetković, "Source coding with quantized redundant expansions: Accuracy and reconstruction," in *Proc. Data Compression Conf.*, Snowbird, UT, 1999, pp. 344–353.

[2] ——, "Properties of redundant expansions under additive degradation and quantization," *IEEE Trans. Inform. Theory*, submitted for publication.

[3] Z. Cvetković and M. Vetterli, "On simple oversampled A/D conversion in $L^2(\mathbb{R})$," *IEEE Trans. Inform. Theory*, vol. 47, pp. 146–154, Jan. 2001.

[4] N. T. Thao and M. Vetterli, "Reduction of the mse in r-times oversampled A/D conversion from $O(1/r)$ to $O(1/r^2)$," *IEEE Trans. Signal Processing*, vol. 42, pp. 200–203, Jan. 1994.

[5] M. Vetterli , V. K. Goyal, and N. T. Thao, "Quantized overcompleted expansions in $\mathbb{R}^N$: Analysis, synthesis and algorithms," *IEEE Trans. Inform. Theory*, vol. 44, pp. 16–31, Jsn. 1998.

[6] J. Kovacević, K. Goyal, and M. Vetterli, "Quantized frame expansions as source-channel codes for erasures using tight frame expansions," in *Proc. Data Compression Conf.*, Snowbird, UT, 1998, pp. 326–335.

[7] V. K. Goyal and J. Kovacević, "Quantized frame expansions with erasures," *Appl. and Comp. Harmonic Anal.*, to be published.

[8] D. Hubel and T. Wiesel, "Receptive fields, binocular interaction and functional architecture in the cat's visual cortex," *J. Physiol.*, vol. 160, pp. 106–154, 1962.

[9] ——, "Brain mechanisms of vision," *Scientific Amer.*, 1979.

[10] W. Freeman E, W. Simoncelli, and D. Heeger, "Shiftable multiscale transforms," *IEEE Trans. Inform. Theory*, vol. 38, pp. 587–602, Mar. 1992.

[11] B. Beferull-Lozano and A. Ortega, "Coding techniques for oversampled steerable transforms," in *Int. Asilomar Conf. Signals, Systems and Computers*, vol. 2, 1999, pp. 1198–1202.

[12] W. Bennett, "Spectra of quantized signals," *Bell Syst. Tech. J.*, vol. 27, pp. 446–472, 1948.

[13] R. M. Gray and T. G. Stockham, "Dithered quantizers," *IEEE Trans. Inform. Theory*, vol. 39, pp. 805–812, May 1993.

[14] I. Daubechies, *Ten Lectures on Wavelets*. Philadephia, PA: SIAM, 1992.

[15] D. Youla, "Mathematical theory of image restoration by the method of convex projections," in *Image Recovery Theory and Application*, H. Stark, Ed. New York: Academic, 1987.

[16] Z. Cvetković and I. Daubechies, "Single-bit oversampled A/D conversion with exponential accuracy in the bit-rate," in *Proc. Data Compression Conf.*, Snowbird, UT, 2000, pp. 343–352.

[17] S. Hein and A. Zakhor, "Theoretical and numerical aspects of an svd-based approach to bandlimiting finite extent sequences," *IEEE Trans. Signal Processing*, vol. 42, pp. 1227–1230, May 1994.

[18] ——, "Reconstruction of oversampled bandlimited signals from sigma delta encoded binary sequences," *IEEE Trans. Signal Processing*, vol. 42, pp. 799–811, Apr. 1994.

[19] S. Rangan and V. K. Goyal, "Recursive consistent estimation with bounded noise," *IEEE Trans. Inform. Theory*, vol. 47, pp. 457–464, Jan. 2001.

[20] B. Beferull-Lozano and A. Ortega, "Construction of low complexity regular quantizers for overcomplete expansions in $\mathbb{R}^N$," in *Proc. Data Compression Conf.*, Snowbird, UT, 2001, pp. 193–202.

[21] ——, "Efficient quantization for overcomplete expansions in $\mathbb{R}^N$," in *Proc. Int. Conf. Acoustics, Speech and Signal Processing*, vol. 6, Salt Lake City, UT, 2001, pp. 3901–3904.

[22] N. J. A. Sloane and B. Beferull-Lozano, "Quantizing using lattice intersections," *J. Discr. Comput. Geom.*, to be published.

[23] J. H. Conway and N. J. A. Sloane, *Sphere Packings, Lattices and Groups*. New York: Springer-Verlag, 1998.

[24] E. M. Rains J, H. Conway, and N. J. A. Sloane, "On the existence of similar sublattices," *Canad. J. Math.*, vol. 51, no. 6, pp. 1300–1306, 2000.

[25] I. J. Good and R. A. Gaskins, "I. J. Good and R. A. Gaskins," *Numerical Math.*, vol. 16, pp. 343–359, 1971.

[26] G. L. Nemhauser and L. A. Wolsey, *Integer and Combinatorial Optimization*. New York: Wiley-Interscience, 1999.

[27] Y. Kitaoka, *Arithmetic of Quadratic Forms*. Cambridge, U.K.: Cambridge Univ. Press, 1993.

[28] O. T. O'Meara, *Introduction to Quadratic Forms*. Berlin, Germany: Springer-Verlag, 1971.

[29] A. V. Geramita and J. Seberry, *Orthogonal Designs: Quadratic Forms and Hadamard Matrices*. New York: Marcel Dekker, 1979.

[30] C. C. MacDuffee, *The Theory of Matrixes*. New York: Chelsea, 1946.

[31] R. Manduchi, G. M. Cortelazzo, and G. A. Mian, "Multistage sampling structure conversion of video signals," *IEEE Trans. Circuits Syst. Video Technol.*, vol. 3, pp. 325–340, Oct. 1993.

[32] J. P. Ward, *Quaternions and Cayley Numbers*. Norwell, MA: Kluwer, 1997.

[33] N. J. A. Sloane S, N. Diggavi, and V. A. Vaishampayan, "Design of asymmetric multiple description lattice vector quantizers," in *Proc. Data Compression Conf.*, Snowbird, UT, 2000, pp. 490–499.

[34] J. H. Conway and N. J. A. Sloane, "Fast quantizing and decoding algorithms for lattice quantizers and codes," *IEEE Trans. Inform. Theory*, vol. IT-28, pp. 227–232, Mar. 1982.

[35] N. T. Thao and M. Vetterli, "Lower bound on the mean-squared error in oversampled quantization of periodic signals using vector quantization analysis," *IEEE Trans. Inform. Theory*, vol. 42, pp. 469–479, Mar. 1996.

[5] Notice that $\theta \in]0, \frac{\pi}{2}[$, which means that $\sin(2\theta) > 0$.

[36] V. Goyal and J. Kovacević, "Optimal multiple description coding of Gaussian vectors," in *Proc. Data Compression Conf.*, Snowbird, UT, 1998, pp. 388–397.

[37] P. Chou, S. Mehrotra, and A. Wang, "Multiple description decoding of overcomplete expansions using projections onto convex sets," in *Proc. Data Compression Conf.*, Snowbird, UT, 1999, pp. 72–81.

[38] A. Petraglia and S. K. Mitra, "High-speed A/D conversion incorporating a QMF bank," *IEEE Trans. Instrum. Meas.*, vol. 41, pp. 427–431, June 1992.

[39] J. Franca, A. Petraglia, and S. K. Mitra, "Multirate analog-digital systems for signal processing and conversion," *Proc. IEEE*, vol. 85, pp. 469–479, Feb. 1997.